AGU PUBLICATIONS

JGR

Journal of Geophysical Research: Earth Surface

RESEARCH ARTICLE
10.1002/2017JF004250

Key Points:
- Algorithm uses a training data set to objectively select and measure river knickzones as bounded reaches of sustained high channel steepness index
- Algorithm-selected knickzones confirm ~80–90% of 178 manually selected knickzones on 1 to 30 m DEMs, and the measured height of confirmed knickzones matches to >90%
- Algorithm is embedded in a set of automated scripts and can be applied to any region with DEM coverage

Supporting Information:
- Supporting Information S1

Correspondence to:
A. B. Neely,
abn5031@psu.edu

Citation:
Neely, A. B., B. Bookhagen, and D. W. Burbank (2017), An automated knickzone selection algorithm (KZ-Picker) to analyze transient landscapes: Calibration and validation, *J. Geophys. Res. Earth Surf.*, *122*, doi:10.1002/2017JF004250.

Received 14 FEB 2017
Accepted 16 MAY 2017
Accepted article online 22 MAY 2017

An automated knickzone selection algorithm (KZ-Picker) to analyze transient landscapes: Calibration and validation

A. B. Neely[1], B. Bookhagen[2,3], and D. W. Burbank[1,3]

[1]Department of Earth Science, University of California, Santa Barbara, California, USA, [2]Institute of Earth and Environmental Science, Universität Potsdam, Postdam, Germany, [3]Earth Research Institute, University of California, Santa Barbara, California, USA

Abstract Streams commonly respond to base-level fall by localizing erosion within steepened, convex knickzone reaches. Localized incision causes knickzone reaches to migrate upstream. Such migrating knickzones dictate the pace of landscape response to changes in tectonics or erosional efficiency and can help quantify the timing and source of base-level fall. Identification of knickzones typically requires individual selection of steepened reaches: a process that is tedious and subjective and has no efficient means to measure knickzone size. We construct an algorithm to automate this procedure by selecting the bounds of knickzone reaches in a χ-space (drainage-area normalized) framework. An automated feature calibrates algorithm parameters to a subset of knickzones handpicked by the user. The algorithm uses these parameters as consistent criteria to identify knickzones objectively, and then the algorithm measures the height, length, and slope of each knickzone reach. We test the algorithm on 1, 10, and 30 m resolution digital elevation models (DEMs) of six catchments (trunk-stream lengths: 2.1–5.4 km) on Santa Cruz Island, southern California. On the 1 m DEM, algorithm-selected knickzones confirm 93% of handpicked knickzone positions (n = 178) to a spatial accuracy of ≤100 m, 88% to an accuracy within 50 m, and 46% to an accuracy within 10 m. Using 10 and 30 m DEMs, accuracy is similar: 88–86% to ≤100 m and 82% to ≤50 m (n = 38 and 36, respectively). The algorithm enables efficient regional comparison of the size and location of knickzones with geologic structures, mapped landforms, and hillslope morphology, thereby facilitating approaches to characterize the dynamics of transient landscapes.

Plain Language Summary The shape of rivers reflects the environments that they flow through and the environments that they link together: mountains and oceans. Anywhere along the length of a river, changes in environmental conditions are propagated upstream and downstream as the river changes its morphology to match the new environmental conditions. Commonly, rivers steepen as land uplifts faster in regions of high tectonic convergence. The steepening of river gradients is propagated upstream and can be mapped to trace zones of high tectonic activity across landscapes and estimate the source and timing of environmental change. Such insights may indicate regions where earthquakes have become more frequent in the recent past and how rivers respond to these changes. In this submission, we detail an algorithm that can use digital topographic data (similar to google earth), to automatically map and measure anomalously steep river reaches across continental scales. This technology can highlight areas that have experienced recent sustained changes in environmental conditions, evident by changes in the morphology of rivers. Such environmental conditions could be changes in tectonic uplift and earthquake activity, changes in sea level, changes in land-use, or changes in climate, all factors that can produce measurable differences in river morphology over time.

1. Introduction

One of the primary goals of geomorphology is to understand how topography records histories of tectonic deformation, climatic forcing, and erosional conditions. Within this framework, landscapes are generally classified as steady state or transient [*Kirby and Whipple*, 2012]. Steady-state landscapes exist where topography is adjusted such that rock uplift is balanced by hillslope lowering and river incision, with an erosional efficiency dictated by climate, rock strength, and erosional process. In contrast, transient landscapes exist where an abrupt and/or sustained change in tectonic or erosional conditions has occurred, such that erosion does not balance tectonics and topography progressively adjusts [*Whipple and Tucker*, 1999; *Whipple*, 2001;

Tucker and Whipple, 2002; *Kirby and Whipple*, 2012; *Whittaker*, 2012]. In a steady-state landscape, the balance between erosion, rock uplift, and erosional efficiency allows topographic metrics such as slope, curvature, or relief to be correlated with current environmental conditions: climate, tectonics, and rock strength. In transient landscapes, topographic form is progressively adjusting, and topographic metrics reveal contrasts between regions that are adjusting to current environmental conditions versus "relict landscapes" that are adjusted to past environmental conditions.

Many conceptual models and field investigations into the mechanics of bedrock incision and hillslope evolution are rooted in assumptions that a landscape is in a steady state, such that topography remains relatively steady in order to transport a steady supply of material without changing landscape morphology [e.g., *Gilbert*, 1909; *Heimsath et al.*, 1997; *Snyder et al.*, 2000; *DiBiase et al.*, 2010]. The solutions obtained from modeling and studying steady-state systems are commonly transferable to analogous steady-state landscapes: landscapes where tectonic and climatic forcing have been steady for an interval longer than the time required to translate landscape responses to a given forcing throughout an entire catchment [*Whipple*, 2001]. Although geomorphic processes and rates are increasingly studied and quantified within steady-state landscapes, the identification and interpretation of transient landscapes still contains many uncertainties [*Whipple*, 2009; *Whittaker and Boulton*, 2012; *Whipple et al.*, 2013; *Godard et al.*, 2013*; Scherler et al.*, 2015].

In transient erosional landscapes, rates of river incision commonly do not match rock uplift rates throughout a catchment. Such landscapes usually originate from a rapid change in downstream base level and an imbalance in sediment supply between relict and adjusting stream reaches [*Whipple and Tucker*, 1999; *Gasparini et al.*, 2006]. Changes in climate may also produce an imbalance between rock uplift and erosion, but climate controls on rates of base-level fall are less clear, as climate-driven changes in channel incision rate may propagate downstream from changes in precipitation or sediment supply in stream headwaters [*Wobus et al.*, 2010; *Moon et al.*, 2011]. Yet, in many cases, transient conditions can be clearly attributed to a variety of other events that trigger accelerated base-level fall. These events can include increased slip rates on faults [*Whittaker et al.*, 2007; *Kirby and Whipple*, 2012], recent stream-capture [*Prince et al.*, 2011; *Willett et al.*, 2014], changes in relative sea level [*Bishop et al.*, 2005], beach-cliff erosion [*Mackey et al.*, 2014], submarine landslides [*Lamb et al.*, 2007], formation of landslide dams [*Korup*, 2006], and rapid drainage of lakes or seas [*Muller*, 1977; *Loget and Van Den Driessche*, 2009]. If an event causes the rate of base-level fall to increase, a steeper, convex topographic step forms in the longitudinal stream profile at the discontinuity between different incision regimes.

Downstream from the convexity, a stream reach adjusts to the new rate of base-level fall [*Whipple*, 2001] and a progressively changing sediment flux as the convexity migrates upstream [*Gasparini et al.*, 2007]. Upstream from the convexity, stream reaches are adjusted to relict environmental conditions prior to base-level fall, as long as divide migration is negligible [*Whipple et al.*, 2017]. This convex step that separates adjusting and relict landscapes is called a knickzone (or knickpoint, if described by a discrete point) [e.g., *Whipple and Tucker*, 1999; *Crosby and Whipple*, 2006]. The presence of knickzones can be used to identify parts of a landscape that are likely still in disequilibrium, and the distribution of knickzones can be used to identify approximately when, where, and how many times a significant change in base-level has occurred.

Knickzones migrate upstream unless an active fault or a resistant geologic unit sustains a locally steepened reach [e.g., *Brocard and Van der Beek*, 2006; *Wobus et al.*, 2006b; *Marshall and Roering*, 2014]. Upstream knickzone migration into relict topography occurs because rapidly eroding reaches produced by increased rates of base-level fall migrate upstream into more slowly eroding relict topography [*Whipple and Tucker*, 1999]. The rate of knickzone migration dictates how quickly base-level changes are propagated upstream and the amount of time needed for a landscape to approach a steady state with respect to the new base-level, tectonic, or climatic forcing.

Multiple studies highlight strong variations in style and pace of knickzone retreat and, thus, the evolution of landscapes toward steady state [*Harbor et al.*, 2005; *Loget and Van Den Driessche*, 2009; *Jansen et al.*, 2011; *Whittaker and Boulton*, 2012; *DiBiase et al.*, 2015; *Shobe et al.*, 2016; *Brocard et al.*, 2016]. Simple stream-power models of knickzone retreat [e.g., *Crosby and Whipple*, 2006] may inadequately describe transient response to base-level fall in these landscapes, (1) because erosional processes acting in steep knickzone reaches are not well represented by stream-power models derived for graded reaches with low bed slopes [*Seidl and Dietrich*, 1992; *Seidl et al.*, 1994; *Lamb et al.*, 2015] or (2) because feedbacks can occur between channel incision,

hillslope response, sediment supply, and drainage-divide migration during knickzone propagation [*Willett et al.*, 2014; *Attal et al.*, 2015; *DiBiase et al.*, 2015; *Shobe et al.*, 2016; *Whipple et al.*, 2017]. These observations stress the importance of understanding the mechanics of knickzone retreat and how these processes vary between different landscapes.

2. Automating Selection of Knickpoints and Knickzones

2.1. Utility of a Knickzone Selection Algorithm to Study Transient Landscapes

One pathway forward lies in the analysis of spatially extensive, topographic data sets where knickzones are contextualized within different landscapes that contain diverse geologic structures, lithologic properties, and hydrologic regimes. Identifying and describing knickzones is greatly aided by the recent proliferation of digital elevation models (DEMs), from which algorithms can extract longitudinal stream profiles. Yet knickzones are usually still selected manually by identifying the bounds of each convex reach of an individual stream profile [*Whipple et al.*, 2007]. This technique has enabled many studies to investigate fundamental connections between patterns of rock uplift, river incision, and landscape response to environmental change [e.g., *Kirby and Whipple*, 2012], but individual knickzone selection within this workflow is notably tedious and subjective and typically provides no consistent method to measure knickzone dimensions, such as height, length, or slope. Such knickzone dimensions set the boundary conditions for local incision and sediment transport [*Meyer-Peter and Müller*, 1948; *Howard and Kerby*, 1983; *Seidl and Dietrich*, 1992], and knickzone size may hold valuable information pertaining to the amount of base-level fall experienced [e.g., *Whittaker and Boulton*, 2012] or patterns of rock strength and knickzone retreat process [e.g., *Lamb and Dietrich*, 2009]. The inability to locate, contextualize, and describe the morphology of knickzones quickly, consistently, and accurately limits our ability to confidently interpret these features and understand how incision within steep knickzone reaches sets the rate and style of landscape response to environmental change.

To address this challenge, we developed an algorithm (KZ-Picker) that uses objective criteria and four adjustable parameters to rapidly locate and measure the dimensions of knickzones from a DEM. The increasing availability and spatial coverage of higher-resolution topographic data have created an opportunity for widespread application of DEM-based algorithms [*Hurst et al.*, 2012; *Fisher et al.*, 2013; *Schwanghart and Scherler*, 2014; *Mudd et al.*, 2014; *Clubb et al.*, 2014; *Purinton and Bookhagen*, 2017]. Implemented largely independent of individual judgment, such algorithms rapidly characterize landscape geometries and aid in developing testable hypotheses for landscape evolution. Similar algorithms have been developed to identify knickzones or reaches of high channel steepness index (k_s or k_{sn} if normalized by a fixed reference concavity) in stream networks [*Whipple et al.*, 2007; *Gonga-Saholiariliva et al.*, 2011; *Schwanghart and Scherler*, 2014; *Mudd et al.*, 2014; *Queiroz et al.*, 2015], but these approaches either do not include a straightforward method to define an appropriate knickzone scale or do not directly measure knickzone geometry.

Here we describe an algorithm specifically designed to select knickzones, and we provide a Matlab™ code that builds on existing TopoToolbox functions [*Schwanghart and Scherler*, 2014]. The algorithm (1) delineates a consistent size and steepness scale suitable for knickzone identification in the context of a particular landscape, study goals, and DEM resolution; (2) uses these criteria to objectively identify and measure the dimensions of knickzone reaches; and (3) compares the accuracy of these automated selections to measurements made manually on each knickzone feature. Our goal has been to create a robust tool with user-friendly parameters that efficiently locates and measures knickzones in any region with DEM coverage. Ideally, a rich contextualization of knickzones within a variety of tectonic, climatic, and lithologic settings will enable future targeted studies that characterize the mechanics of incision operating within knickzones and address the significance of these features in driving landscape evolution.

2.2. Definition of Knickzones and Knickpoints

Empirical evidence suggests that streams equilibrated to steady base-level rise or fall rates, uniform climate conditions, and uniform bedrock strength throughout a catchment commonly exhibit a form that can be fit by a power-law relationship between local channel slope and contributing drainage area [*Hack*, 1957; *Flint*, 1974]:

$$S = k_s \cdot A^{-\theta}, \tag{1}$$

where S is local channel slope, A is contributing drainage area, k_s is channel-steepness index, and θ is the

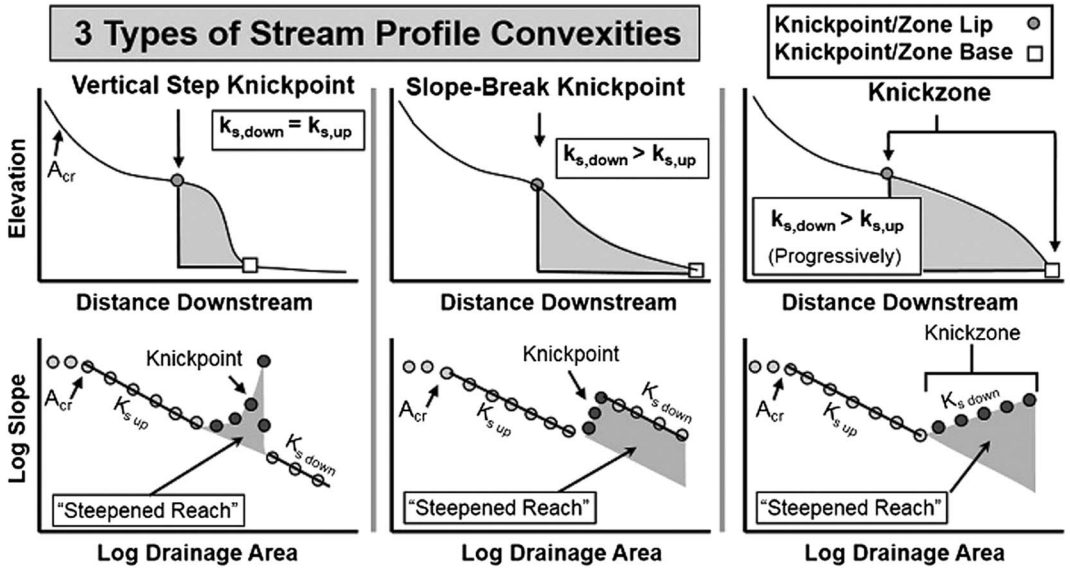

Figure 1. For simplicity, we use the term "knickzone" to describe all convexities found in stream profiles, because all three convexity types exhibit a steepened zone (gray) where the local channel-steepness index is elevated over the average channel-steepness index of the full profile (bottom). (top) Profiles are plotted in distance/elevation space and (bottom) log area/log slope space. The critical area, A_{cr}, highlights a change in the log area/log slope relationship that typically defines a transition between colluvial streams and the fluvial network [Modified after *Lague,* 2014].

concavity index, which typically ranges between 0.35 and 0.6 in steady-state landscapes [*Kirby and Whipple*, 2012]. Knickpoints or knickzones mark localities where stream gradients are steeper than expected for the respective contributing drainage area, thereby creating a positive deviation, or convexity, on a log(A)/log(S) plot (Figure 1) [*Howard et al.*, 1994; *Whipple and Tucker*, 1999]. These convexities could be locally steepened zones, such as waterfalls [*Baldwin et al.*, 2003; *Bishop et al.*, 2005; *Mackey et al.*, 2014], or could define a sustained change in the power-law relationship between channel slope and drainage area, shown through an increase in k_s (channel-steepness index) or k_{sn} (channel-steepness index calculated with a fixed θ value) [*Crosby and Whipple*, 2006; *Wobus et al.*, 2006a; *Harkins et al.*, 2007; *Berlin and Anderson*, 2007; *Miller et al.*, 2012; *Miller et al.*, 2013; *DiBiase et al.*, 2015].

Conventionally, locally steepened zones are called "vertical step knickpoints" if the channel-steepness index is identical upstream and downstream of a convexity (Figure 1). If the channel-steepness index experiences a sustained increase downstream from a convexity, the convexity is called a "slope-break knickpoint" [*Kirby and Whipple*, 2012]. If multiple knickpoints are spaced closely together or a knickpoint diffuses during upstream migration, a "knickzone" can form where the channel-steepness index progressively increases toward the mouth of a stream or the next downstream confluence with a larger channel (Figure 1) [*Lague*, 2014]. Factors controlling whether a convexity will be a vertical-step knickpoint, slope-break knickpoint, or knickzone are complex and likely reflect the perturbation that originally generated the convexity as well as interactions between erosional processes within the convexity, bedrock lithology, and whether the stream is transport or detachment limited [*Tucker and Whipple*, 2002; *DiBiase et al.*, 2015].

Because of the steepened nature of vertical-step knickpoints, slope-break knickpoints, and knickzones, bedrock steps can be much more abundant in these stream reaches, and erosional mechanisms such as plucking, toppling, block sliding, and plunge-pool drilling are commonly enhanced [*Howard et al.*, 1994; *Weissel and Seidl*, 1997; *Whipple et al.*, 2000; *Haviv et al.*, 2010; *Lamb and Dietrich*, 2009; *Dubinski and Wohl*, 2013]. Additionally, channel width and properties, such as sediment cover, grain size, and bed roughness, change markedly in most knickpoints and knickzones, thereby affecting sediment transport and bedrock incision occurring in these reaches [*Haviv et al.*, 2006; *Whittaker et al.*, 2007; *Fisher et al.*, 2013; *DiBiase et al.*, 2015; *Lamb et al.*, 2015]. Although differing from prior terminology, we refer to all steepened reaches that are more likely to exhibit the characteristics listed above as "knickzones," because these reaches have a lip and a base that mark the start and end of a reach that is steeper than the average channel-steepness index of the full profile.

2.3. Using χ Plots to Objectively Identify Knickzones: Algorithm Construction

Our "knickzone" algorithm (KZ-Picker) is designed to locate the lips and corresponding bases of knickzones in longitudinal stream profiles (Figure 1). Once these knickzone boundaries are located, the algorithm can measure the height, length, and slope of the knickzone reach. The knickzone-selection algorithm uses a χ-plot visualization of a longitudinal stream profile to aid knickzone identification [*Royden et al.*, 2000; *Perron and Royden*, 2013]. Here we present a brief review of how a χ-plot is derived, along with an explanation of why this representation is useful in automated knickzone selection.

A χ-plot is constructed by integrating the stream-power equation: a common approach used to model fluvial erosion in uplifting landscapes. In the stream-power model, change in elevation at a position along a stream is modeled as rock uplift minus fluvial incision:

$$\mathrm{d}z/\mathrm{d}t = U(x,t) - K(x,t)\cdot A(x,t)^m\cdot|\mathrm{d}z/\mathrm{d}x|^n, \tag{2}$$

where z is elevation, t is time, x is position along a longitudinal stream profile, U is the rock uplift rate, K is a constant relating erosional efficiency to rock strength, sediment bedload, and climatic factors, A is upstream drainage area, m is a constant relating drainage area to discharge and catchment geometry, and n is a constant relating channel slope to erosional efficiency [*Howard and Kerby*, 1983; *Whipple and Tucker*, 1999]. Assuming a steady state ($\mathrm{d}z/\mathrm{d}t = 0$) and isolating $\mathrm{d}z/\mathrm{d}x$, integration of equation (2) with respect to upstream position yields

$$z(x) = z(x_\mathrm{b}) + (U/(K\,A_0{}^m))^{1/n}\chi, \tag{3}$$

where the variable

$$\chi = \int_{xb}^{x} (A_0/A(x))^{m/n}\mathrm{d}x, \tag{4}$$

for which x_b is the x position of base level, $z(x_\mathrm{b})$ is the elevation at local base level, and A_0 is a reference drainage area used to compare relative changes in drainage area [see *Perron and Royden,* 2013, for full derivation]. The m/n ratio equals θ or the concavity index (equation (1)). Both empirical data [*Howard and Kerby*, 1983] and theoretical predictions where erosion depends on bed shear stress [*Whipple and Tucker*, 1999] suggest that m/n typically lies between 0.35 and 0.6 in detachment-limited streams. The stream-power model simplifies bedrock-stream erosion in a number of ways, mainly by excluding direct equations that model the physics of erosional mechanisms, namely plucking and abrasion [*Whipple et al.*, 2000; *Sklar and Dietrich*, 2001, 2004; *Chatanantavet and Parker*, 2009]. Nevertheless, the stream-power model can be used generally as a predictive reference to identify deviation from steady-state stream profile form, as is typical for knickzones.

Given uniform rock uplift, rock strength, and climate conditions within a catchment, an m/n value derived from a linear fit to equation (3) will collapse a stream network (including all tributary profiles) onto a line in χ-elevation space, with $z(x_\mathrm{b})$ as the y intercept and $(U/(K\cdot A_0{}^m))^{1/n}$ as the slope of the line for increasing χ. Note that $(U/(K\cdot A_0{}^m))^{1/n} \propto k_\mathrm{s}$ (channel steepness index), because A_0 is an arbitrary reference constant used to scale the χ axis [*Whipple and Tucker*, 1999; *Perron and Royden,* 2013]. Hence, the slope of the line in χ/elevation space represents the channel steepness index (k_s). See *Perron and Royden* [2013] for a complete list of advantages and disadvantages when using a χ-plot representation of a stream profile.

The largest advantage of using a χ-plot representation for automated knickpoint selection is the removal of a stream's natural concavity [*Hack*, 1957; *Flint*, 1974] and an expected linear relation of graded streams in elevation/χ space, where χ is a measure of distance scaled for progressive changes in upstream drainage area along a longitudinal profile (Figure 2a). Choice of a representative m/n ratio is required to remove the concavity of the trunk stream and tributaries. If the trunk stream and all tributaries exhibit this m/n ratio, these streams will all collapse around a linear profile when transforming from distance-elevation space to χ-elevation space [*Perron and Royden*, 2013]. The transformation of a longitudinal profile to χ-elevation space permits detrending of a stream profile relative to a linear profile drawn in χ-elevation space from the channel mouth to the channel head (Figures 2b–2c). This linear profile represents a steady-state profile with a constant channel-steepness index needed to span the relief and length of the stream. The residual between a stream's observed χ profile and this linear profile represents the deviation from a graded stream profile with uniform uplift and erosional efficiency. We plot this residual as a "detrended χ-plot." Such plots explicitly

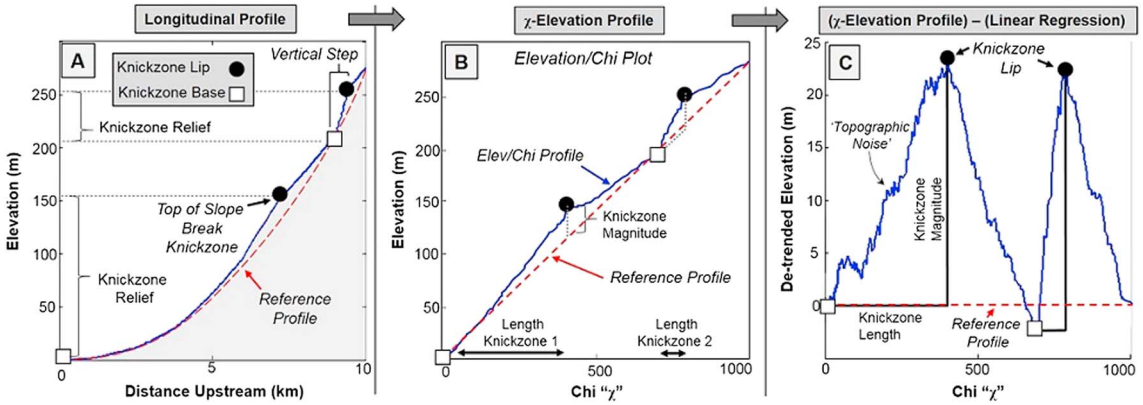

Figure 2. (a) Example longitudinal stream profile. Knickzone lips and bases are marked. The elevation drop across each knickzone is the knickzone relief. An *m*/*n* ratio must be chosen for the reference profile, which spans the length and relief of the stream. (b) Transformation of stream longitudinal profile into χ-space. Slope of the reference profile connecting the stream outlet to headwaters (red-dashed line) represents the average channel-steepness index, k_s, for the given *m*/*n* ratio. (c) A detrended χ-plot represents the elevation residual between the stream profile and the linear reference profile in χ-elevation space. Knickzone lips plot as local maxima, and knickzone bases plot as local minima. Knickzone magnitude is the detrended elevation drop between the knickzone lip and corresponding knickzone base.

reveal where the channel steepness index is "understeepened" (negative slope: Figure 2c) or "oversteepened" (positive slope: Figure 2c) with respect to a theoretical "reference" graded stream profile spanning the length and relief of the catchment.

At inflections from understeepened reaches to steepened reaches, local maxima in a detrended χ-plot represent potential knickzone lips that are at a maximum elevation relative to the reference profile, and at inflections from steepened reaches to understeepened reaches, local minima represent potential knickzone bases that are at a minimum elevation relative to the reference profile (Figure 2c). We exploit these two points to define the bounds of a knickzone (Figures 2a–2c). The difference between (i) the observed elevation loss between the bounds of the knickzone and (ii) the loss predicted by the slope of the reference profile defines the "magnitude" of the knickzone (Figure 2c).

2.4. Choosing an *m*/*n* Ratio for χ-Transformation in Transient Streams

A common approach for χ-plot construction is to iterate through all *m*/*n* combinations and use the *m*/*n* ratio that best linearizes the χ-elevation profile of the stream network to the trunk stream [*Perron and Royden*, 2013; *Mudd et al.*, 2014; *Schwanghart and Scherler*, 2014]. If tributaries exhibit an *m*/*n* ratio different from the trunk stream, these tributaries will produce a curved plot in χ-elevation space. Tributaries with an *m*/*n* ratio higher than the trunk stream will be concave up in χ-elevation space, and tributaries with an *m*/*n* ratio lower than the trunk stream will be convex in χ-elevation space (see Figures S8 and S9 in the supporting information for examples). Such effects will, respectively, diminish or amplify the magnitude of tributary knickzones.

In steady-state streams, *m*/*n* is typically well constrained between 0.35 and 0.6, but in transient streams, *m*/*n* can fall well outside this range and vary spatially throughout a catchment [*Whipple et al.*, 2013; *Mudd et al.*, 2014]. Either the *m*/*n* ratio that linearizes the χ-elevation profile of the trunk stream can be calculated directly, although perhaps reflecting a transient value if the stream profile is in disequilibrium, or a reference *m*/*n* ratio between the empirical ranges of steady-state *m*/*n* values can be assumed (0.45 is a common value). The choice of *m*/*n* sets the concavity of the reference (graded) stream when converting to χ-elevation space. All tributaries and the trunk stream are linearized relative to this profile, and therefore, all knickzones are measured relative to this reference profile. If a fixed *m*/*n* value is used for all basins, knickzones represent reaches of anomalously high k_{sn}, and if the reference *m*/*n* value varies between basins, knickzones represent reaches of anomalously high k_s [*Kirby and Whipple*, 2012].

In our analysis, we calculate the *m*/*n* ratio directly as the value that linearizes the χ-elevation profile of the trunk stream. We note basin-to-basin variability of *m*/*n* in channel profiles that presumably represent transient morphologies and compare how the choice of *m*/*n* affects knickzone selection. Although differing from

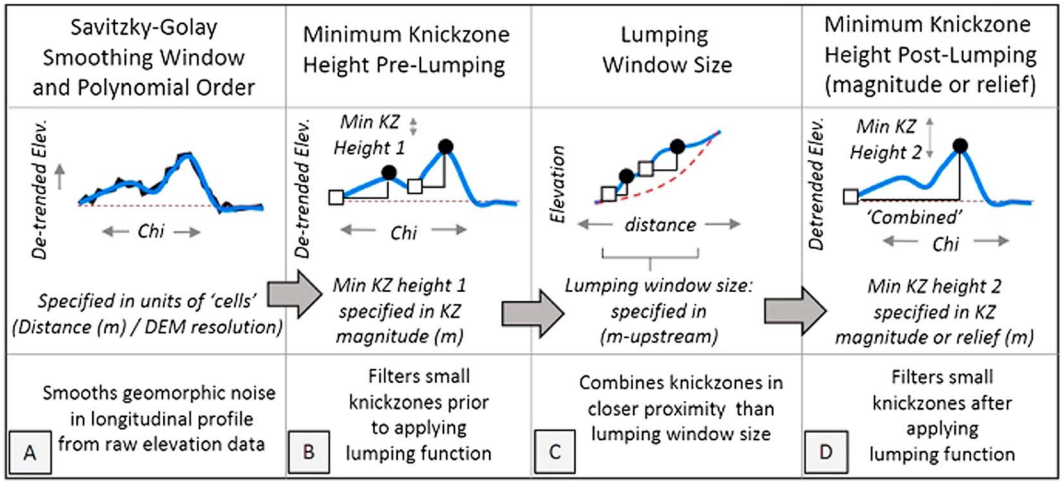

Figure 3. Illustrated sequence of smoothing and filtering parameter functions on a convex reach. The (a) convex reach represents a significant knickzone that is larger than (d) *Min KZ Height 2*, but composed of two smaller steps that are spaced closer than (c) *Lumping window size* and each larger than (b) *Min KZ Height 1*. (c) *Lumping window size* must be recorded in distance upstream-space and not χ-space, because the scaling of χ will change between catchments of differing *m*/*n* ratio (equation (4)).

our methodology, if *m*/*n* values of trunk streams fall far from the range of typical values for steady-state streams, we suggest a fixed *m*/*n* value (0.45 for example) should be chosen. A fixed *m*/*n* value will define a reference stream profile with a fixed concavity, and this profile geometry will be used to detrend the concavity of all streams and tributaries throughout all basins (dashed red line in Figure 2). If available, nearby steady-state streams with similar rock type, tectonics, and climate forcing can be used to inform estimates of an appropriate fixed *m*/*n* value for the reference steady-state stream profile.

2.5. Algorithm Parameters Needed to Define Knickzone Scale

Our use of a detrended χ-elevation profile represents knickzone reaches as sustained deviations from the average channel-steepness index. A series of four smoothing and filtering functions, as described below, are applied to the detrended χ-profile to smooth topographic noise and objectively select knickzones. These smoothing and filtering functions ensure that the algorithm only selects deviations of a scale appropriate for the knickzone scale of interest (Figure 3). Similar approaches are used to measure the amplitude and scale of roughness elements along topographic profiles [*Smith*, 2014]. Because knickzones of interest may change scale according to the total landscape relief, to the goals of an analysis, or to the resolution of a DEM, these smoothing and filtering functions are flexible and can be calibrated using known knickzone positions and dimensions.

First, the longitudinal profile is filtered with a Savitzky-Golay filter [*Orfanidis*, 1996]. The Savitzky-Golay filter fits a polynomial of specified degree to a chosen smoothing window size to remove high-frequency noise in the stream longitudinal profile resulting from DEM interpolation or fine-scale topography: for example, the surface of boulders in channels (Figure 3a). The polynomial fit used by the Savitzky-Golay filter preserves sharp but sustained changes in stream gradient around knickzone lips and bases that would be smoothed by standard moving average filters. The degree of smoothing can be adjusted by changing the smoothing window size. The polynomial order of the filter must be less than the smoothing window size, so in lower resolution DEMs that require less smoothing, a lower order polynomial must be used. Otherwise, we find that a constant polynomial order is appropriate to smooth longitudinal profiles, and we only adjust the smoothing window size which effectively changes the ratio between the polynomial order and the number of cells used to smooth the profile.

Subsequently, the magnitude of each convex reach is compared to a specified minimum knickzone magnitude. Convex reaches with magnitudes smaller than this threshold are removed (Figure 3b). This minimum knickzone magnitude reflects a user-specified minimum height of individual steps or waterfalls and excludes small changes in detrended riverbed elevation that are not removed by the Savitzky-Golay filter.

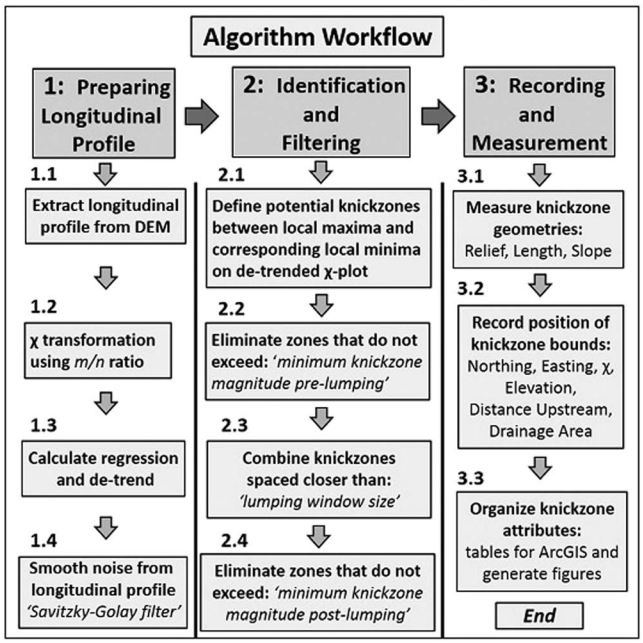

Figure 4. Workflow and use of parameters within the algorithm. Each processing step is represented by a gray box. (top) Main functions are represented by dark gray boxes, and subfunctions within these steps are represented by light gray boxes. Parameters are indicated in italics in the box where the parameter is used.

Commonly, a full knickzone comprises multiple steps or closely spaced waterfalls [*Howard et al.*, 1994; *DiBiase et al.*, 2015]. To select a full knickzone instead of individual waterfalls, a lumping function searches in the streamwise direction for knickzones that are spaced in close proximity to one another. If the knickzone lip and knickzone base of two adjacent steps are spaced closer than the lumping-window size, the knickzones are combined, and the new bounds of the knickzone span from the upstream-knickzone lip to the downstream-knickzone base (Figure 3c). The lumping-window size (m) should reflect the spacing of bedrock steps and small waterfalls within knickzones in a landscape, which may be qualitatively known from prior field experience. The lumping function combines small, closely spaced bedrock steps or waterfalls into larger, landscape-scale knickzone features.

After running the lumping function, knickzone magnitudes are compared to a second minimum knickzone magnitude of a specified value, and knickzones smaller than this threshold value are discarded (Figure 3d). The parameters, smoothing-window size, minimum knickzone magnitude prelumping, lumping-function window size, and minimum knickzone magnitude postlumping, set the scale of convex features that are considered to be significant knickzones. Importantly, we allow flexibility in these parameter values and the ability to calibrate these parameters to a training data set, because the definition of a relevant knickzone may change according to specific study goals, the relief of a particular landscape, or the resolution of a DEM (as discussed in detail in later sections).

After performing the filtering and smoothing functions, the algorithm records statistics for convexities identified as knickzones (Figure 4). These statistics include the northing, easting, elevation, distance upstream from drainage outlet, and contributing drainage area of each knickzone's lip and base. Additionally, the algorithm compares the knickzone lip and base position to calculate the knickzone's length (m), relief (m), magnitude (m), and slope (Figure 2a). The knickzone magnitude (m) records the amount of relative oversteepening through the reach with respect to the average channel-steepness index through the same reach (Figures 2b and 2c). The knickzone relief (m) measures the elevation drop across the knickzone interval (Figure 2a).

The user can specify whether filtering small convexities should be based on a minimum knickzone relief or knickzone magnitude. Knickzone relief is a more intuitive measurement that can be compared directly to observations of waterfall height or base-level fall in the field, but in a concave longitudinal profile, knickzones occurring farther upstream are inherently steeper and thus have a higher knickzone relief. Knickzone magnitude is insensitive to this bias, because natural stream concavity is detrended when magnitude is measured (Figure 2c).

2.6. Algorithm Treatment of Slope-Break Knickpoints

Stream reaches downstream from slope-break knickpoints (Figure 1) are steepened relative to the entire stream profile and adjust to a slope that is needed to match the new rock uplift rate or erosional efficiency [*Whipple*, 2001] and temporal changes in sediment flux as the slope-break knickpoint continues to migrate

into the relict reach upstream [*Gasparini et al.*, 2007]. In the case of slope-break knickpoints, our algorithm extends a knickzone from the lip at the slope-break knickpoint to the base located at the mouth of the stream or a downstream confluence with a larger channel (Figures 1 and 2). The amount of base-level fall is not directly calculated by the algorithm through the measured magnitude or relief of the knickzone but could be calculated by comparing the modern base-level elevation to the extrapolation of an upstream-relict longitudinal profile based on its concavity and channel-steepness index [*Schoenbohm et al.*, 2004; *Clark et al.*, 2006; *Harkins et al.*, 2007; *DiBiase et al.*, 2015]. If the entire steepened reach downstream from a slope-break knickpoint is bounded by a knickzone, the measured knickzone relief represents the amount of base-level fall, *plus* the amount of vertical migration experienced by the knickzone lip. If a reach downstream from a slope-break knickpoint consists of multiple vertical-step knickpoints, knickzones will be selected over each steepened step.

The knickzone magnitude measures the elevation difference between the knickzone lip and base after removing the amount of elevation drop over the same interval expected given the channel steepness of the reference profile used for detrending (Figure 2c). This measurement is sensitive to changes in the m/n ratio when comparing between stream networks, because the m/n ratio influences the relative length of the stream segments upstream and downstream from the knickzone lip in χ-space and therefore also influences the average channel steepness measured from the channel head to the stream outlet or confluence (equation (4)). Unlike knickzone magnitude, knickzone relief is less sensitive to the value of the m/n ratio, because knickzone relief measurements are not made relative to the average channel steepness of the stream.

It is important to note that within one basin or if a fixed m/n value is used, knickzone magnitude serves as a useful measurement to identify oversteepened reaches [*Gasparini et al.*, 2007]. For example, given two catchments of equal drainage area responding to the same acceleration in base-level fall, knickzone lips would sit at the same elevation given an ideal stream-power response. If upstream migration is stalled in one catchment relative to an ideal stream-power response [e.g., *Wobus et al.*, 2006c; *Crosby et al.*, 2007], a hanging valley forms upstream from the stalled knickzone lip, and the knickzone reach downstream from the lip will be oversteepened. The knickzone lip in the hanging valley catchment will (i) sit at a higher detrended elevation relative to the average channel steepness used to detrend the χ-plot and (ii) record a larger knickzone magnitude (Figure S1) [e.g., *Brocard et al.*, 2016]. This dependence makes knickzone magnitude a useful measure to identify variations in response style between different basins responding to base-level fall events.

As a caveat, our approach is less likely to identify a slope-break knickpoint inset within the reach downstream from another slope-break knickpoint. This situation can occur if a stream experiences an increased rate of base-level fall followed by subsequent increase in the rate of base-level fall [*Whittaker et al.*, 2007]. Our approach is more likely to identify only the uppermost significant slope-break knickpoint and to extend a knickzone through the downstream reach. Use of a segment-fitting algorithm [e.g., *Mudd et al.*, 2014] might be a more appropriate approach to analyze such a situation.

3. Application of Algorithm to Catchments on Santa Cruz Island, California

3.1. Geologic Setting, DEM Processing, and Longitudinal Profile Construction

We test the performance of the knickzone selection algorithm (KZ-picker) on DEMs of Santa Cruz Island (SCI), California, which is located ~36 km west of Ventura, California, and is the largest of the California Channel Islands (~250 km^2). Total relief on Santa Cruz Island is ~740 m, and most streams are between 1 and 18 km in length. Santa Cruz Island is actively uplifting at rates of ~0.1 mm/yr [*Pinter et al.*, 1998; *Muhs et al.*, 2014] and displays features commonly associated with fluvial knickpoints: coastal terraces, hanging valleys, and steep hillslopes with exposed bedrock cliffs and mass-wasting scars.

Importantly, high-resolution lidar aerial surveys span all of the California Channel Islands and allow for generation of $<$1 m resolution DEMs (2010 US Geological Survey Channel Islands Lidar Collection). We generate a bare-earth DEM with 1 m spatial resolution based on a lidar point cloud with an average point density of ~10 pts/m^2. A minimum drainage area (A_{cr}) of 10^5 m^2 was used to approximate the break between hillslope-colluvial reaches and fluvial channels [*Montgomery and Foufoula-Georgiou*, 1993]. The 1 m resolution DEM permits use of a relatively small minimum drainage area [*Clubb et al.*, 2014], and slope-area plots confirm

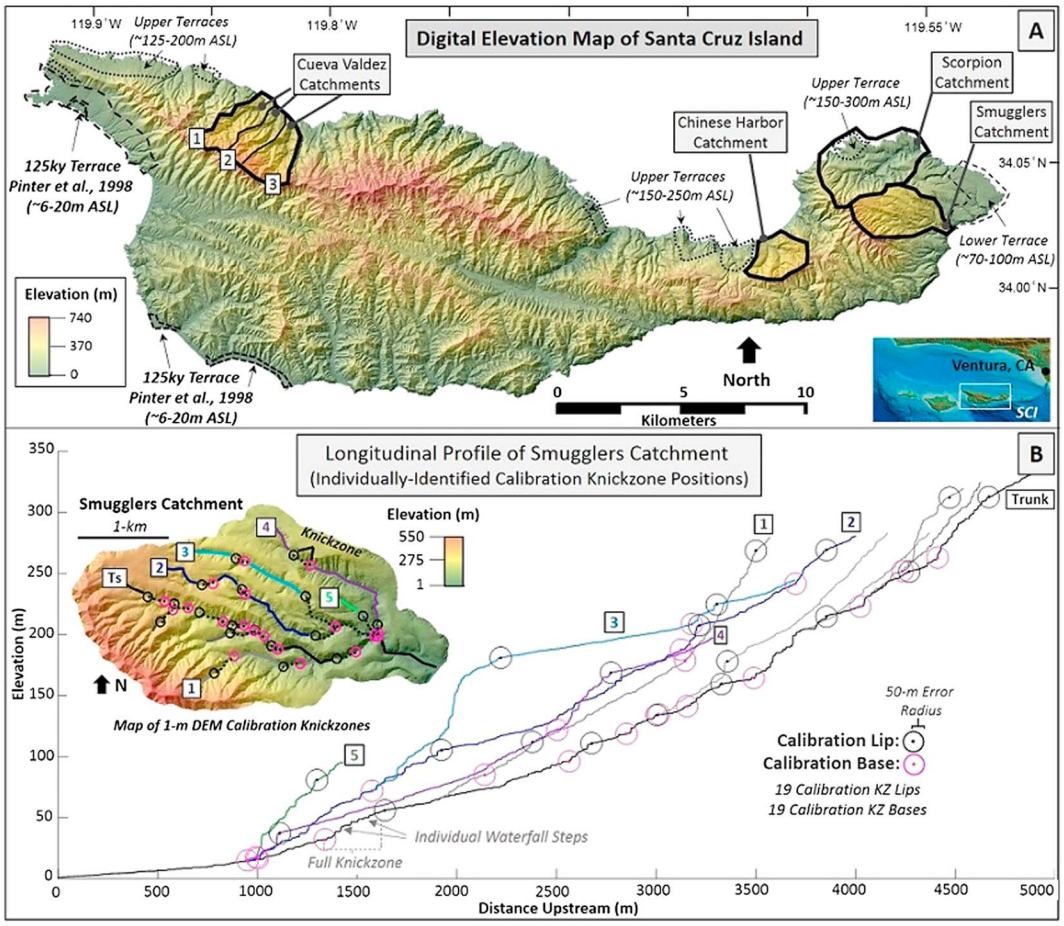

Figure 5. (a) Elevation map of Santa Cruz Island, California, shows position of catchments analyzed (outlined in bold). Extensive marine terraces are labeled; dated terraces are in bold [*Pinter et al.,* 1998]. (b) Longitudinal profiles of Smugglers Catchment streams are marked with 19 calibration knickzone bases and 19 calibration knickzone lips. This catchment was used to calibrate best-fit smoothing and filtering parameter values. Major tributary branches are labeled and colored. We assume a 50 m error radius that surrounds each calibration knickpoint selection. Inset: 1 m DEM of Smugglers catchment with spatial distribution of knickzones (lips in black connected with black dashed line to bases in pink).

that 10^5 m^2 typically marks the transition to a linear decreasing log-area/log slope relationship in SCI catchments (Figure S2). In order to assess algorithm performance on lower DEM resolutions that are more widely available, this 1 m DEM was bilinearly resampled to 10 m point spacing using the average elevation of a 10 × 10 block containing 100 one-meter cells. This process was repeated using a 30 × 30 block containing 900 one-meter cells to bilinearly resample the 1 m DEM to 30 m point spacing. These resampled DEMs simulate lower resolution coverage (10 and 30 m resolution) of the same topography.

We selected six coastal catchments to test the performance, sensitivity, and optimization of parameters for different DEM resolutions (Figure 5a). Catchments range from 1.7 to 6.1 km^2 and contain knickzones, some likely related to uplifted marine terraces and resistant bedrock units. Precise knowledge of knickzone origin, however, remains a subject for future work and is not necessary for our analysis, which aims only to identify these features using the automated algorithm. A field survey and GPS data point collection was conducted on the northwestern terrace of SCI to verify the existence of easily accessible knickzones identified on the 1 m DEM (Figure S3).

For each basin, m/n ratio was calculated as the value that best linearizes the catchment network to the trunk stream. This m/n ratio and a reference area $A_0 = 10^6$ m^2 are used together to transform each stream profile into χ-space. Although reflecting a mix of transient and relict terrains, we also calculate basin-wide channel steepness index in each catchment. Two calculations of channel steepness index are made with

TopoToolbox. The first calculation uses a fixed m/n ratio (we use 0.45) and fits a nonlinear least squares regression through the median of binned log-slope log-area data (100 bins) [*Schwanghart and Scherler*, 2014]. The second calculation fits a linear regression to the χ-elevation profile to calculate k_s (k_{sn} if the m/n ratio is held fixed) [*Schwanghart and Scherler*, 2014]. Both techniques calculate the channel steepness index, but gridding artifacts are amplified when calculating slopes in a slope-area regression, and log-binned slope-area data require a different regression technique than χ-elevation data [*Perron and Royden*, 2013; *Schwanghart and Scherler*, 2014; *Wang et al.,* 2017]. Differences between calculated k_{sn} derived from using a log(S)/log(A) regression and from a χ-elevation regression are explored in section 4.3.

In each catchment, calibration knickzone positions were visually identified from the 1 m DEM by individually selecting the bounds of knickzone reaches. Manual selections were made directly on longitudinal stream profiles (Figure 5b) with guidance from a calculated slope-area plot [*Whipple et al.*, 2007]. We attempted to keep knickzone scale as consistent as possible during manual selection, but we recognize that some inconsistency is unavoidable given the subjective nature of manual knickzone selection, and therefore, our calibration data set is imperfect. Knickzone lips marked the upstream extent of broadly convex reaches, whereas knickzone bases marked the downstream extent of broadly convex reaches. Calibration knickzones were selected to span over 100 m scale convex reaches and have a minimum of ~4 m of additional relief relative to the reference channel steepness.

The calibration knickzones selected using the 1 m DEM are assumed to reflect the real position of knickzone features. To assess algorithm performance on lower resolution DEMs, calibration knickzones are also selected using longitudinal profiles derived from 10 m and 30 m resolution DEMs. The bounds of sharp topographic breaks, such as knickzones, change as lower resolution DEMs progressively smooth topography. Small ($<$20 m) knickzones may disappear, and the position of calibration knickzones selected on the 10 m and 30 m DEMs may differ from the position of calibration knickzones selected on the 1 m DEM. We compare the position of calibration knickzones selected on the 10 m and 30 m to the calibration knickzones selected on the 1 m DEM to quantify how lowering DEM resolution may obscure or hide sharp knickzone features relative to their real position on the landscape.

3.2. Criteria Used to Assess the Accuracy of the KZ-Picker Algorithm

To quantify agreement between algorithm-selected knickzone positions and manually selected calibration knickzone positions, we follow a technique that compares the spatial agreement between two data sets of different point positions [*Orlandini et al.*, 2011; *Clubb et al.*, 2014]. The technique relies on an allowable error radius between the points in each data set and tallies the number of "true positives" (TP), "false positives" (FP), and "false negatives" (FN). True positives (TP) are calibration knickzone boundaries that lie within the specified allowable error radius from an algorithm-selected knickzone boundary, false positives (FP) are algorithm-selected knickzone boundaries that lie outside of the allowable error radius for all calibration knickzone boundaries, and false negatives (FN) are calibration knickzone boundaries with no corresponding algorithm-selected knickzone boundaries located within its allowable error radius.

From the tally of these three classifications, we use three metrics to compare the positions of calibration and algorithm knickzones (Figure 6). (1) Reliability totals the number of true positives (TP) relative to the number of false positives (FP) plus the number of true positives. Reliability decreases from a maximum value of "1" (no false positives) as the algorithm selects more spurious (FP) knickzones that do not have corresponding calibration knickzones. (2) Sensitivity totals the number of true positives (TP) relative to the number of false negatives (FN) plus the number of true positives. Sensitivity decreases from a maximum value of "1" (no false negatives) if the algorithm fails to identify knickzones near calibration knickzones. (3) Geometric accuracy calculates the percent error between the relief of TP algorithm-knickzone lips to the relief of corresponding TP calibration-knickzone reaches. Ideally, reliability (R), sensitivity (S), and geometric accuracy (G) should be maximized (= 1) by the algorithm parameters used (see formulas in Figure 6), and these metrics can be used to assess the accuracy of the algorithm relative to a suite of calibration knickzones individually selected by an analyst.

3.3. Finding Best-Fit Parameter Values and Quantifying Parameter Impact

Nineteen calibration-knickzone lips and 19 calibration-knickzone bases were manually identified on the 1 m DEM (Figure 5b) and on the 10 m DEM of the Smugglers Basin catchment. Only 18 calibration-knickzone lips

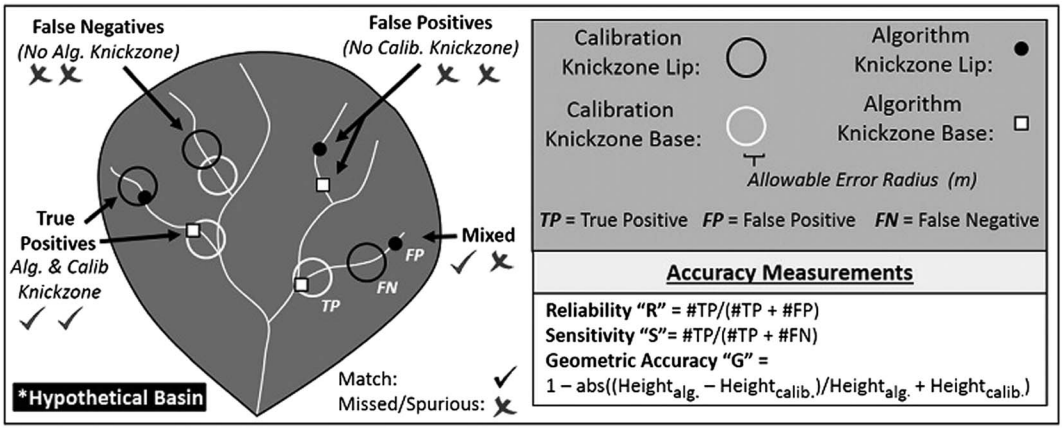

Figure 6. Illustration of reliability, sensitivity, and geometric accuracy criteria used to assess algorithm performance. Algorithm-selected knickzone lips and bases are compared to allowable error circles drawn around calibration knickzone lips and bases. This comparison classifies algorithm and calibration knickzone boundaries as true positives (TP), false positives (FP), and false negatives (FN). These classifications are used to calculate reliability *R*, sensitivity *S*, and geometric accuracy *G* of the algorithm knickzone selections.

and 18 calibration-knickzone bases were manually identified using the 30 m DEM, because decreasing DEM resolution obscures smaller knickzones. For each of the three DEM resolutions, these knickzone bounds were used to calibrate and optimize knickzone selection parameters: (1) Savitzky-Golay smoothing window size (cells), (2) lumping window size (m), (3) minimum knickzone height pre-lumping (m), and (4) minimum knickzone height postlumping (m).

Parameters were systematically varied across the values in Table 1, using an algorithm that loops through different parameter combinations and finds the parameter combination that produces the maximum reliability, sensitivity, and geometric accuracy between algorithm-selected knickzones and calibration knickzones. A spatial error tolerance of 50 m around each calibration knickzone boundary was used to distinguish true positives from false-negatives and false-positives (Figure 6). Although somewhat arbitrary, 50 m was chosen to provide tolerance for knickzones with subtle inflections potentially reflecting drawdown reaches [*Gardner*, 1983] or infill at the base of waterfalls [*DiBiase et al.*, 2015], while minimizing overlapping error tolerance between knickzone boundaries occurring near tributary confluences. The parameter combination producing the highest average reliability (*R*), sensitivity (*S*), and geometric accuracy (*G*) (= Avg. RSG) for both knickzone lips and bases was defined as the suite of best-fit parameter values (Figure 7). This process was repeated on

Table 1. Parameter Value Ranges Used for Calibration, Optimization, and Impact Testing (KZ = Knickzone)[a]

Parameter Name	Parameter Value									
	1 m DEM									
Smoothing window (cells)	11	25	51	75	101	125	151	175	201	225
Savitzky-Golay polynomial order	11	11	11	11	11	11	11	11	11	11
Lumping window (m)	10	25	50	75	100	125	150	175	200	250
Min. KZ height prelumping (m)	0.25	0.5	0.75	1	1.25	1.5	1.75	2	2.25	2.5
Min. KZ height postlumping (m)	1	2	3	4	5	6	7	8	9	10
	10 and 30 m DEM									
Smoothing window (Cells)	3	5	7	9	11	13	17	19	21	23
Savitzky-Golay polynomial order	3	5	7	9	11	11	11	11	11	11
Other parameters are not grid-cell dependent (same as 1 m DEM calibration)										

[a]1 m DEM: Range of parameter values tested: All parameters are varied through 10 possible values, and each combination of smoothing window, lumping window, and minimum knickzone height combination (total of 10,000) is rated by the average of the scored reliability (*R*), sensitivity (*S*), and geometric accuracy (*G*) produced from the set of input parameters (Figure 7). The 10 m and 30 m DEMs require smaller smoothing window sizes. Savitzky-Golay polynomial order was generally held fixed, but lower-order polynomials are required to test smaller smoothing window sizes to avoid oversmoothing coarser DEMs. No smoothing was performed on the input longitudinal profile if the polynomial order matches the smoothing window size (for some of the 10 and 30 m DEM parameter values).

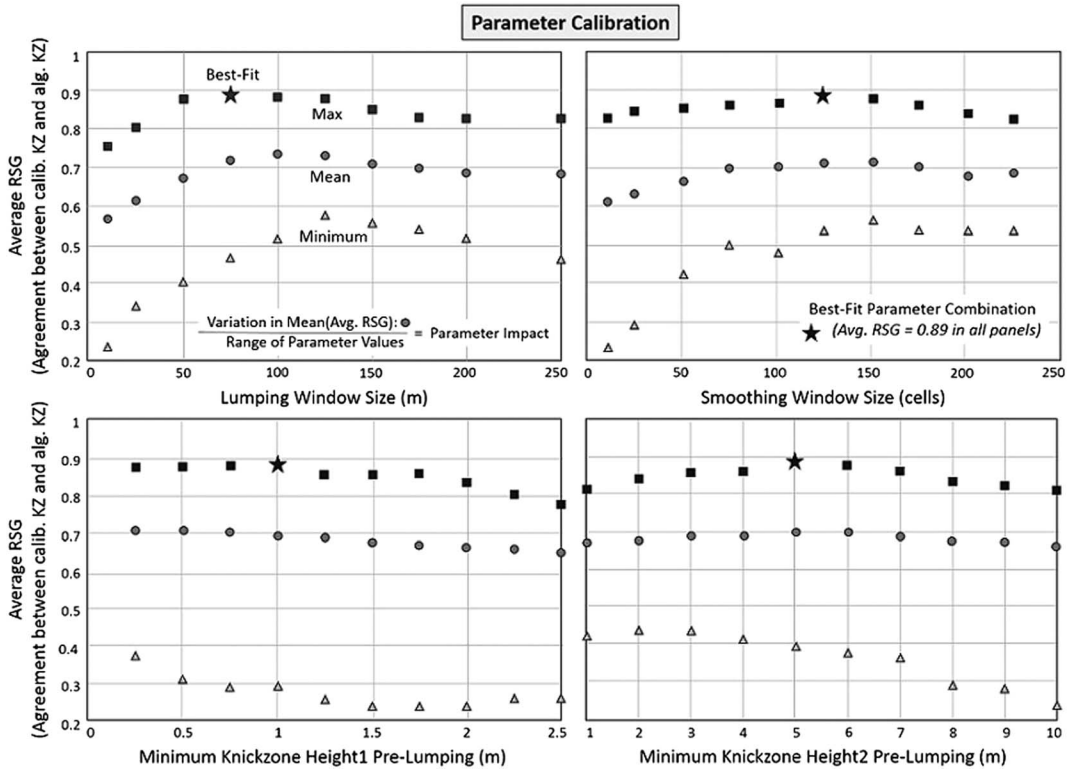

Figure 7. Accuracy of algorithm on 1 m DEM showing range of parameters given in Table 1. The parameter tested and the range of values used are listed on the *x* axis, whereas the *y* axis displays the spread of average-reliability-(*R*)-sensitivity-(*S*)-geometric accuracy (*G*) when varying the other three parameters. The best-fit parameter value in each panel (*black star*) is identified as the parameter values that maximize *R*, *S*, and *G* (highest Avg. RSG). Out of the 1000 combinations for each parameter value, the maximum (*squares*), mean (*circles*), and minimum (*triangles*) Avg. RSG are displayed. Variation in the mean Avg. RSG for each parameter value across the suite of parameter values indicates the parameter impact or how strongly algorithm results are affected by the parameter selection.

the 10 and 30 m resolution DEMs of Smugglers Basin using the calibration knickzones selected from the 10 and 30 m DEMs, respectively.

Subsequently, the parameter impact was recorded as the variance in the mean reliability, sensitivity, and geometric accuracy calculated over the range of a parameter value (the variation of the gray circles in Figure 7). The parameter impact was then cross-correlated with each of the three accuracy measurements: reliability, sensitivity, and geometric accuracy, in order to identify which parameters most strongly affect each accuracy measurement (Figure S4). Two weak correlations were identified: the lumping window (m) exerts a control on the geometric accuracy of knickzone selections (R^2 = 0.25), and the final minimum knickzone height (m) affects the sensitivity (R^2 = 0.21). These dependencies are expected, because the lumping window controls how closely spaced convex steps are combined to match the geometry (*G*) of landscape-scale knickzones. After performing the lumping function, the final minimum knickzone height threshold sets the scale of the smallest knickzone considered in the analysis. If the scale of the smallest calibration knickzone does not match the scale of the smallest algorithm knickzone, either calibration knickzones will be missed and sensitivity (*S*) will decrease, or algorithm knickzones smaller than the calibration knickzones will be selected and reliability (*R*) will decrease. This dependence stresses the importance of keeping consistent selection criteria while mapping calibration knickzones.

3.4. Applying Algorithm With Previously Determined Best-Fit Parameters

Throughout a landscape, the geometry of knickzones may vary among different catchments with differing lithology or base-level histories. After each algorithm parameter was calibrated to maximize the average of reliability, sensitivity, and geometric accuracy in Smugglers Basin (Figure 7), this parameter combination was used to objectively extract knickzone positions in five other study catchments (Chinese Harbor,

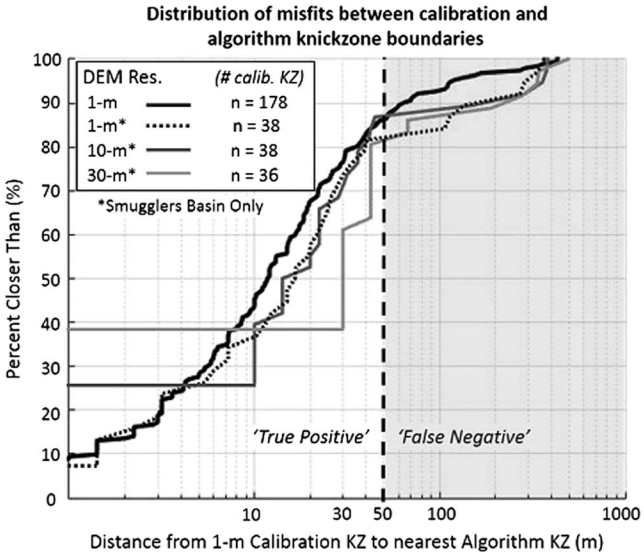

Figure 8. Cumulative distribution of distances from calibration-knickzone lips (or bases) to closest corresponding algorithm-knickzone lip (or base) are plotted for each DEM resolution of Smugglers Basin and including analysis expanded to 1 m DEMs of all six test catchments (n = 178). Distributions are similar for all three DEM resolutions.

Scorpion, and Cueva Valdez 1, 2, 3: see Figure 5a for location). Following the same methodology as Smugglers Basin, algorithm-selected knickzones were compared to calibration knickzones manually selected from the 1 m DEMs of each catchment prior to running the algorithm. We recorded the reliability, sensitivity, and geometric accuracy of algorithm results, along with distances between calibration knickzone lips (or bases) and the nearest corresponding algorithm knickzone lip (or base) to quantify the distribution of errors between the algorithm knickzones and calibration knickzones.

4. Results of Application to Santa Cruz Island

Application-example results are organized into four sections: (1) section 4.1 presents the accuracy of the algorithm relative to all calibration knickzones selected; (2) section 4.2 presents longitudinal profiles of Smugglers Basin and best-fit parameters found for each DEM resolution from the calibration exercise (false negative calibration knickzones are noted and briefly discussed); (3) section 4.3 shows the impact of changing DEM resolution on longitudinal profile analysis and knickzone position; and (4) section 4.4 provides an example of how this algorithm can be used to contextualize knickzones with surrounding landscapes and generate preliminary hypotheses of landscape evolution.

4.1. Algorithm Validation

We identified best-fit input parameter values to verify 178 calibration-knickzone boundaries in six basins on SCI. On the 1 m DEM, the algorithm identifies 93% of all calibration-knickzone lips and bases within a spatial accuracy of ≤100 m, 88% within a spatial accuracy of ≤50 m, and 46% within a spatial accuracy of ≤10 m. Results are similar on the 10 m and 30 m DEMs, which were only quantified in detail in Smugglers Basin (for 10 m DEM, n = 38 calibration-knickzone boundaries; and 30 m DEM, n = 36 calibration-knickzone boundaries). On the 10 m DEM, the algorithm identifies 88% of all calibration-knickzone lips and bases within a spatial accuracy of ≤100 m, 82% within a spatial accuracy of ≤50 m, and 39% within a spatial accuracy of ≤10 m (one grid-cell length). On the 30 m DEM, the algorithm identifies 86% of all calibration-knickzone lips and bases within a spatial accuracy of ≤100 m, 82% within a spatial accuracy of ≤50 m, and 61% within a spatial accuracy of ≤30 m (one grid-cell length) (Figure 8).

Reliability and geometric accuracy remain ≥0.9 in all cases, indicating that the algorithm selected few (<10%) spurious knickzones, and on average, the measured relief of knickzones with true-positive knickzone lips are within 10% of measured relief across calibration knickzones. All spatial accuracy distributions show rapid increase in misfit distance near or slightly above 50 m (the approximate minimum spacing between neighboring tributaries), indicating that the remaining percent of calibration-knickzone lips and bases (~7–18%, depending on DEM resolution) did not have corresponding algorithm-knickzone lips and bases.

In addition to automating and standardizing the selection procedure, algorithm workflow reduces analysis time many fold. Knickzone selection using the algorithm took between 4 and 5 min with the 1 m resolution DEM (~10,000 × 10,000 pixels), whereas individual selection of calibration knickzones required approximately 16 h to complete and compile. The detailed calibration performed in this study provides suitable parameter values for other studies using this algorithm on 1 m, 10 m, and 30 m DEMs (Figure 9 and appendix). It is not

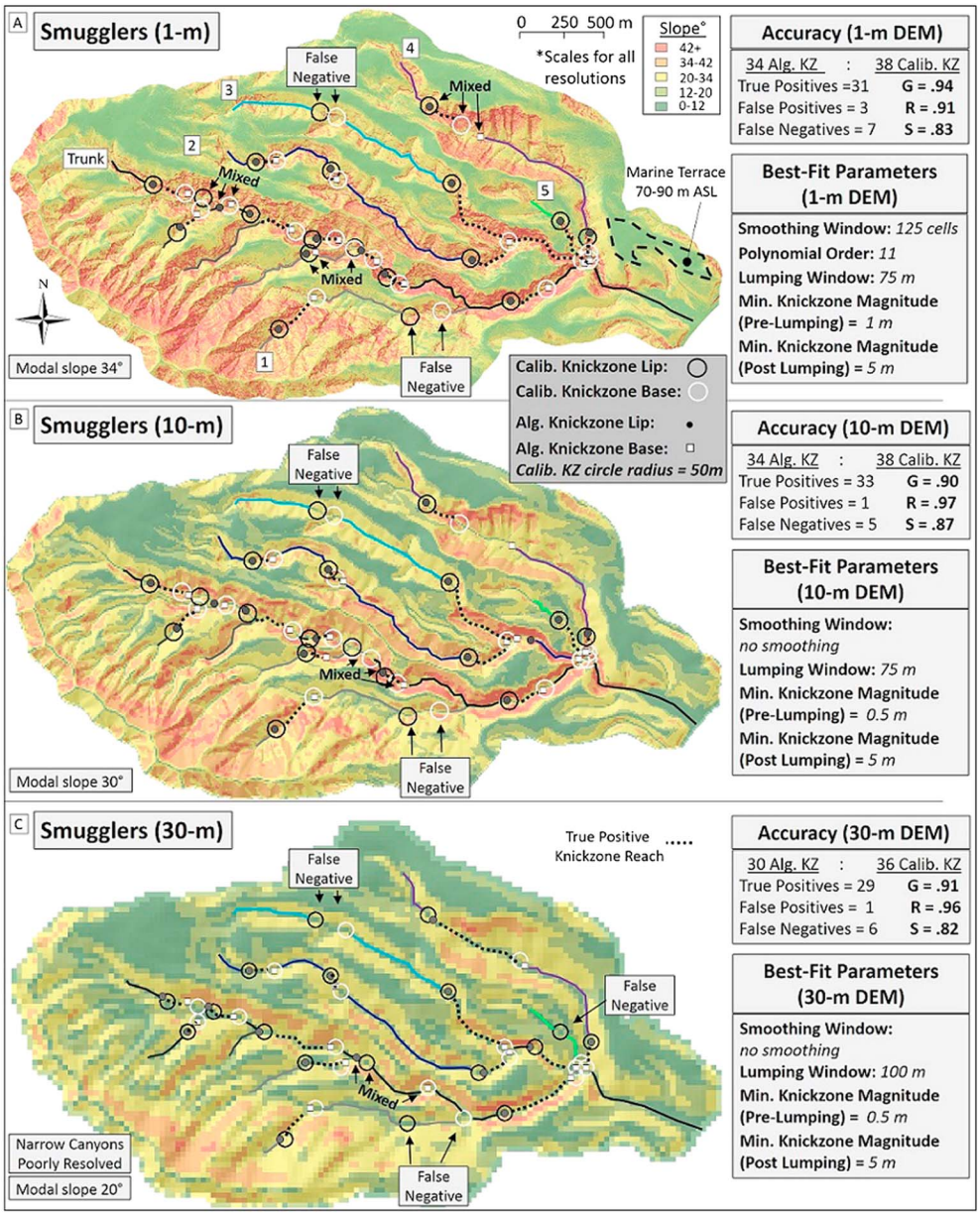

Figure 9. Comparison of algorithm-selected knickzone positions with calibration knickzone positions on 1 m, 10 m, and 30 m DEMs. Accuracy metrics for reliability (*R*), sensitivity (*S*), and geometric accuracy (*G*) are recorded along with best-fit parameter values. Knickzone reaches where algorithm lips and bases match calibration lips and bases are emphasized with dashed black lines. Modal slope decreases (up to ~14°) as lower resolution DEMs smooth topographic roughness, and steep canyons containing knickzones become poorly resolved.

necessary to repeat the parameter calibration steps unless the DEM resolution or desired minimum knickzone scale (~4 m) deviates from values used in this study. Parameter adjustments can be tuned by visually inspecting output longitudinal profiles and approximating necessary adjustments. For example, if many knickzones that are too small are selected, the final minimum knickzone height parameters can be increased. Also, 10–30 m resolution DEMs that are not derived from resampling a higher resolution 1 m DEM may have more noise and may require larger minimum knickzone height thresholds and smoothing window sizes to distinguish knickzones from DEM noise (see Taiwan parameters in appendix). If more precise adjustments are required, the workflow presented in this manuscript can be repeated (see supporting information Section S13). We include a table (see appendix A1) of parameter combinations that performed

well when testing this algorithm on landscapes with different DEM resolution, relief, stream length, and target minimum knickzone heights than SCI.

4.2. Best-Fit Parameter Values and Accuracy Within Smugglers Basin

On the 1 m DEM, distributions of spatial misfit between calibration and algorithm knickzones are similar for all basins (n = 178 knickzone boundaries) and for Smugglers Basin only (n = 38 knickzone boundaries), with a slightly larger fraction of false negatives occurring in Smugglers Basin (Figure 8). Knickzones are plotted in map view and on longitudinal profiles generated from 1, 10, and 30 m DEMs of Smugglers Basin (Figures 9 and 10) and 1 m DEMs of additional calibration catchments (Figures S5–S8). Results are optimized on the 1 m DEM with a Savitzky-Golay smoothing window filter of 125 cells, a lumping window of 75 m, and a final minimum knickzone magnitude of 5 m. Results on both the 10 m and 30 m DEMs are optimized when using no smoothing with the Savitzky-Golay filter, lumping windows of 75 m (~7 cells) and 100 m (~3 cells), respectively, and a final minimum knickzone magnitude of 5 m.

Two calibration knickzones in Smugglers Basin are consistently missed in all DEM resolutions. One knickzone (distance upstream = 3300 m, tributary 3) is located upstream from a very large knickzone in the center of tributary 3 (Figures 9 and 10). Another knickzone (distance upstream = 2200 m, tributary 1) is located downstream from a very large knickzone that extends to the headwaters of tributary 1 (Figures 9 and 10). Very large knickzones dominate the amplitude of the detrended χ-plot of these two tributary profiles, causing the m/n ratio of these tributaries (-0.84, tributary 3; 0.77, tributary 1) to be considerably different from the m/n ratio of the trunk stream (0.49). Much of the relief in these χ-profiles is consumed by single large knickzones, and smaller knickzones superimposed upstream and downstream of these features are missed (Figures S9 and S10). We caution that this effect can generate persistent false negatives regardless of DEM resolution. In this case, both large-amplitude knickzones in tributaries 1 and 3 encompass $>$47% of the total tributary relief: a large fraction compared to the smaller calibration knickzones in the same tributary that were missed and only represent $<$11% of the total tributary relief.

These false negatives seem uncommon but are unavoidable given our identification technique. On all the 1 m DEMs, only 3 out of the total 89 calibration-knickzone lip and base pairs were missed entirely by the algorithm (both lip and corresponding base were false negatives, e.g., Figure 6). The false negatives of tributaries 1 and 3 have clear expression in the output longitudinal profiles. Although not ideal, these knickzones could be manually selected to compliment algorithm results, if these knickzones were essential to provide an interpretation of landscape dynamics.

Importantly, these false negatives highlight the significance of selecting a representative m/n ratio for χ-plot construction and knickzone selection. If the trunk stream displays an m/n ratio that reflects a high state of disequilibrium relative to tributaries, small-magnitude knickzone selections in tributaries with different m/n ratios may be obscured. For these circumstances, we suggest fixing the reference m/n ratio to a value typical in steady-state streams (0.45, for example), rather than allowing the m/n ratio to adjust to a trunk stream that represents a highly transient condition. We explore this effect in Chinese Harbor: a calibration catchment with a nearly convex trunk stream profile, m/n = 0.08 (Figure S11).

4.3. Impact of DEM Resolution on Longitudinal Profile Analysis and Knickzone Position

In lower resolution DEMs ($>$10 m), pixel spacing is coarse, and stream meanders can be shortcut, thereby decreasing channel length, increasing measured channel slope, and possibly generating artefactual knickzones [*Fisher et al.*, 2013; *Perron and Royden*, 2013]. In high-resolution DEMs ($\leq$10 m), sampling may be finer than the channel width and capture meanders between sediment infill in the thalweg of dry streambeds. When decreasing DEM resolution from 1 m to 30 m in the study catchments on SCI, such effects manifest in an 18–30% increase in basin-average k_{sn} when calculated with a log(S)/log(A) regression (Table 2) and a similar decrease in stream length (Figure 10). This effect is smaller when using a χ-elevation regression to calculate k_{sn}, but this resolution-bias should be considered when comparing k_{sn} between analyses that use different DEM resolutions [cf. *Purinton and Bookhagen*, 2017].

In four out of the six basins, a regression in χ-elevation space yields a significantly higher measure of basin-wide k_{sn} than when k_{sn} is measured on a slope-area plot (Table 2 and Figure S12). Sometimes this discrepancy is as large as ~200%, as in the Chinese Harbor catchment. Basins with lower concavities (m/n Chinese

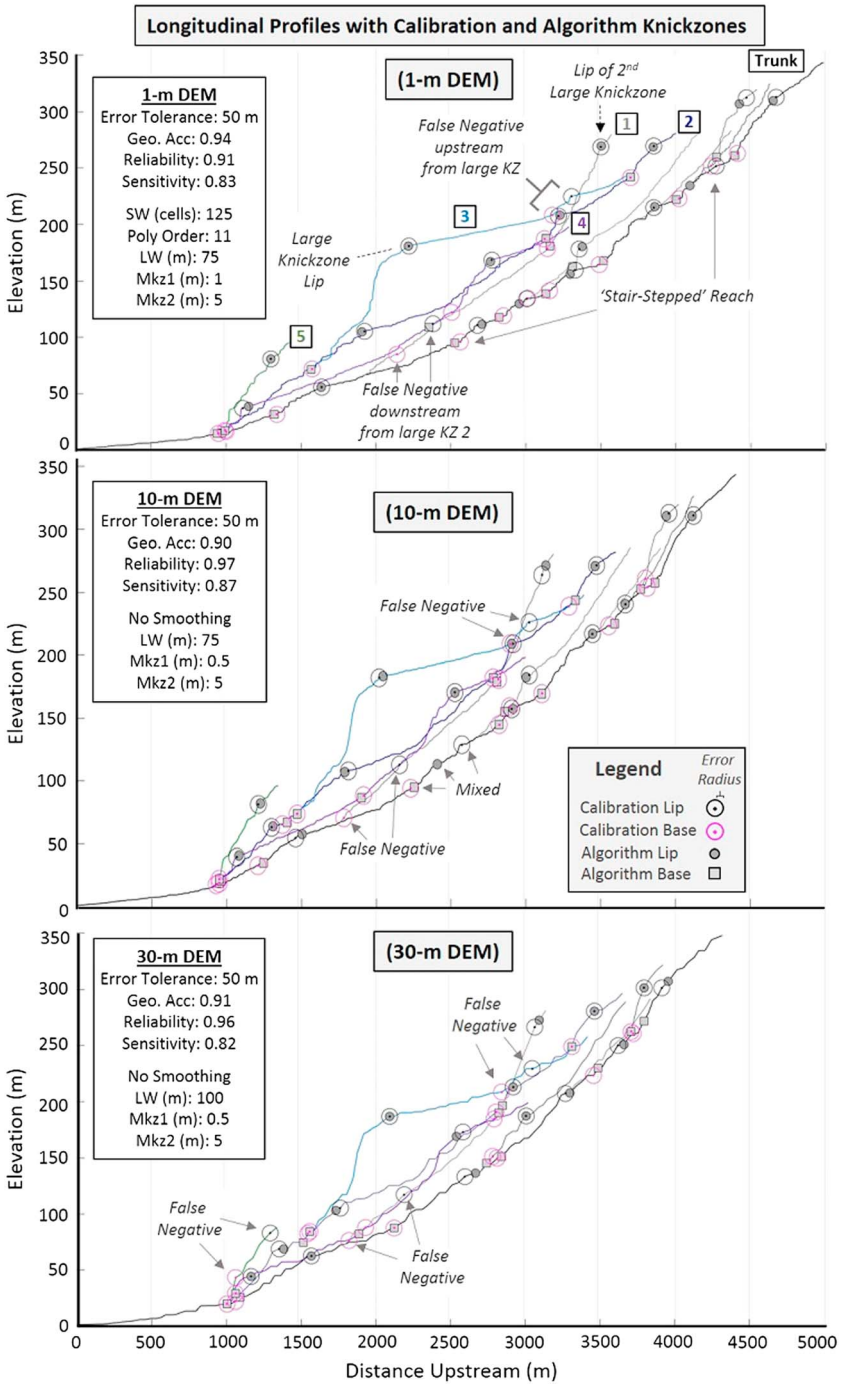

Figure 10. Longitudinal profiles of Smugglers Basin for 1 m, 10 m, and 30 m DEMs (for profile location see Figure 9). (a) Persistent false negatives are noted, and (b, c) additional changes in knickzone selections are highlighted. Figure 10b contains labels for each tributary (cf. Figure 9). Note progressive diffusion of the "stair-stepped" reach as a function of coarser DEM resolution.

Harbor = 0.08) and steeper downstream reaches have higher k_{sn} values when measured using a χ-elevation regression relative to a log(S)/log(A) regression. Potentially, this trend reflects tendencies for regressions based on slope-area data to weight headwater portions of stream networks more heavily relative to regressions using χ-elevation data. Although not the focus of this study, such discrepancies between k_{sn} values

Table 2. Summary of Basin Statistics[a]

DEM Res.	1 m DEM			10 m DEM			30 m DEM		
Basin Name (*Lithology*)	Area (km^2)	*m/n*	k_{sn} (SA),(χ) ($m^{0.9}$)	Area (km^2)	*m/n*	k_{sn} (SA),(χ) ($m^{0.9}$)	Area (km^2)	*m/n*	k_{sn} (SA),(χ) ($m^{0.9}$)
Basin statistics									
Smugglers (V-Sh)	5.23	0.49	(25.7),(33.1)	5.22	0.49	(30.0),(37.4)	5.15	0.45	(32.3),(38.9)
Scorpion (V-Sh)	6.13	0.70	(22.9),(23.7)	6.19	0.66	(25.7),(26.1)	6.15	0.64	(27.4),(28.6)
Chinese Harbor (Sh)	2.70	0.08	(32.4),(62.4)	2.64	0.08	(36.5),(68.6)	2.59	0.03	(39.0),(72.5)
Cueva Valdez 1 (V)	2.50	0.31	(37.7),(54.5)	2.58	0.29	(43.5),(61.8)	2.63	0.31	(47.9),(66.3)
Cueva Valdez 2 (V)	1.70	0.48	(38.6),(55.1)	1.76	0.45	(44.2),(61.7)	1.82	0.44	(50.2),(63.8)
Cueva Valdez 3 (V)	2.60	0.39	(45.0),(61.2)	2.60	0.38	(53.7),(69.4)	2.63	0.37	(53.5),(70.8)
Knickzone selection statistics									
N = # KZ	*R*	*S*	*G*	*R*	*S*	*G*	*R*	*S*	*G*
Smugglers *N* = 38, 38, 36	0.91	0.83	0.94	0.97	0.87	0.90	0.96	0.82	0.91
Scorpion *N* = 58	0.86	0.86	0.90						
Chinese Harbor *N* = 20	0.95	0.95	0.89						
Cueva Valdez 1 *N* = 22	0.91	0.91	0.94						
Cueva Valdez 2 *N* = 14	1.00	1.00	0.96						
Cueva Valdez 3 *N* = 26	0.92	0.88	0.90						
Total mean	0.91	0.88	0.92						

[a]These values are displayed in graphical form in Figure S12. k_{sn}(SA),(χ) refers to k_{sn} calculated with a log(*S*)/log(*A*) regression and χ-plot regression, respectively (*m/n* fixed at 0.45). *R*, *S*, and *G* refer to reliability, sensitivity, and geometric accuracy of algorithm knickzone selections, respectively. Knickzone calibration on 10 m and 30 m DEMs was only performed in Smugglers Basin. (*V*) = SCI Andesite and Dacite, (*Sh*) = Monterey shale.

calculated from a slope area plot and those calculated using a χ-elevation plot should be further investigated and considered when comparing topometrics between studies using different techniques to calculate k_{sn} [e.g., *Wang et al.*, 2017].

Change in stream length and smoother topography with coarser DEM resolution will change the position and visibility of knickzone features [*Duvall et al.*, 2004]. Sharp knickzone lips and bases will be smeared across greater distances at coarser resolutions, and small-magnitude knickzones may be potentially obscured ($<$ ~10–20 m). We reselected separate sets of calibration knickzones on each DEM resolution of Smugglers Basin to analyze algorithm performance specifically, even if the input DEM is a poor representation of the actual topography. We quantify the inaccuracy due to the use of the 10 m and 30 m DEMs for manual knickzone identification analysis by calculating the spatial misfit between the calibration knickzone boundaries located on coarser DEMs and the calibration knickzones selected on the 1 m DEM, which are interpreted to represent the "real" (or "true") location of knickzone boundaries.

In particular, small steps and drawdown reaches are sampled differently on each DEM, because coarser DEMs may sample channel banks, rather than the stream thalweg. Most channels in this study have valley bottoms $<$10 m wide. Knickzone boundaries generally move on the order of tens of meters when coarsening DEM resolution (Figures 11a and 11b, tributaries 1, 2, and 3), but some calibration knickzones with misfits larger than 100 m are likely undetectable on coarser DEMs. Such effects are pronounced in the trunk stream of Smugglers Basin, where a high-resolution DEM is needed to resolve steep canyon walls and abrupt waterfall steps (Figures 9, 11a (trunk), and 11b).

4.4. Example of Applying KZ-Picker to Transient Landscape Analysis: Chinese Harbor Catchment

In conjunction with aerial photographs or other DEM calculations (slope and curvature), the results of the algorithm can be used to form initial interpretations and testable hypotheses. During our calibration exercise, we hypothesize strong coupling between knickzone retreat and hillslope failures that have occurred within the Chinese Harbor catchment in northeast SCI. In this catchment, uplifted marine terraces indicate long-term, relative base-level fall of at least 200 m. Knickzone lips cluster strongly around two separate elevation intervals. The correlation between knickzones, eustatic sea level changes [*Snyder et al.*, 2002], sea cliff retreat [*Mackey et al.*, 2014], and the timing of terrace formation is unclear, but the clustering of knickzones at common elevation intervals is a prediction of the stream-power model when forced with pulsed or oscillatory

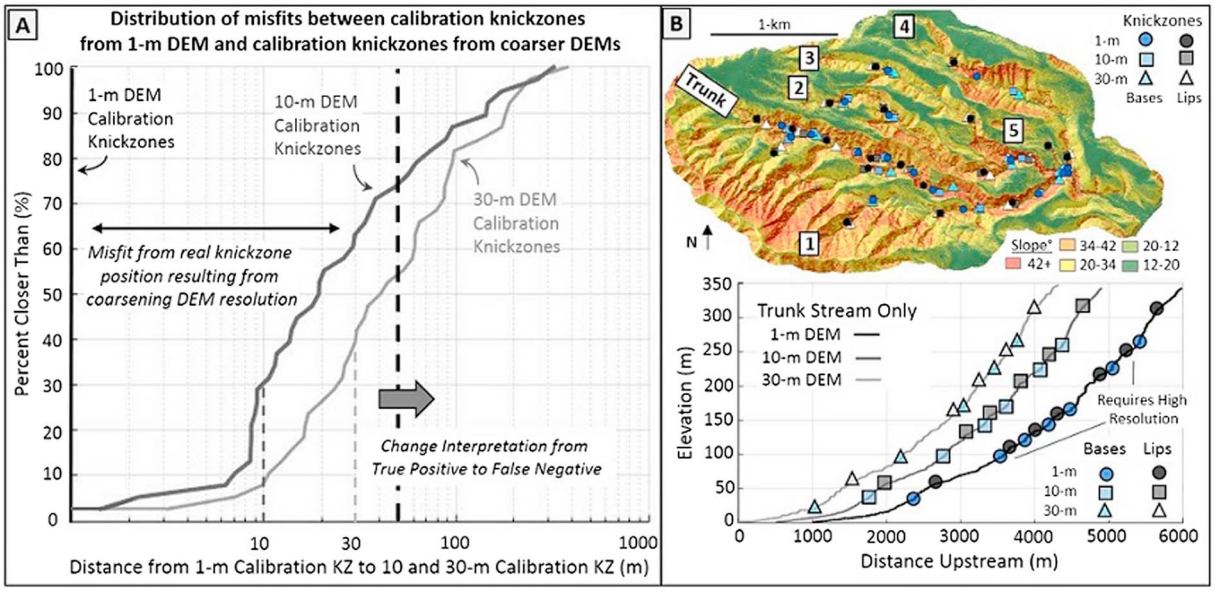

Figure 11. (a) Coarsening DEM resolution generates considerable misfit between 1, 10, and 30 m calibration knickzones (minimum knickzone magnitude ~4 m). (b) Longitudinal profile of trunk stream and map of Smugglers Basin plot differences in calibration knickzone boundaries for each DEM resolution. Trunk stream longitudinal profiles are horizontally offset by 500 m.

base-level fall [*Niemann et al.,* 2001; *Royden and Perron*, 2013]. Such base-level forcing would be expected in an uplifting coastal landscape.

Additionally, knickzones of similar elevation in the Chinese Harbor catchment are not fixed to a single resistant bed or lithologic unit. Bedrock units are folded along a northwest-plunging syncline with limbs dipping 10–40° [*Weaver and Nolf*, 1969]. For radially distributed knickzones observed in the Chinese Harbor catchment to fixate on a single lithologic unit following this structure, knickzones would have to occur at significantly lower elevations if positioned further away from the fold axis or down-plunge. However, knickzones are positioned at similar elevations throughout the catchment, implying that bedrock lithology does not exert a dominant control on knickzone position (Figure 12).

Combined with the slope-map and airphoto imagery, we note a high abundance of landslide headscarps in hillslopes downstream from a wave of knickzones that occur in all tributaries at ~150–200 m above sea level. A large landslide has dammed the westernmost tributary and partially filled the longitudinal stream profile (Figure 12). Most large landslides slip in the direction of bedrock dip. Under assumptions that knickzone retreat rate increases with larger contributing drainage area [*Crosby and Whipple*, 2006; *Berlin and Anderson*, 2007], the lower knickzone interval is migrating faster than the upper knickzone interval; therefore, the middle knickzone interval is more rapidly debuttressing steep hillslopes and priming these hillslopes for landslide failure [e.g., *Golly et al.*, 2017].

With targeted fieldwork to quantify the mobility of these knickzones [e.g., *Mackey et al.*, 2014], one could use this setting to study the interaction between transient channel incision and hillslope response. Hillslope properties, such as slope, bedrock composition/orientation, landslide prevalence, and soil/vegetation cover, may have direct links to channel incision, likely governed here by knickzone retreat rate and knickzone height. Such preliminary insights are revealed by the spatial coverage of the KZ-Picker, which effectively contextualizes knickzone position and geometry with surrounding landscape attributes. Notably, most initial interpretations, such as those described above, would require further analysis and fieldwork to adequately test specific hypotheses.

5. Discussion

Our algorithm presented here efficiently contextualizes the position and geometry of knickzones within the spatial distribution of known geologic structures, lithologic units, and hillslope morphologies (Figures 9 and 12).

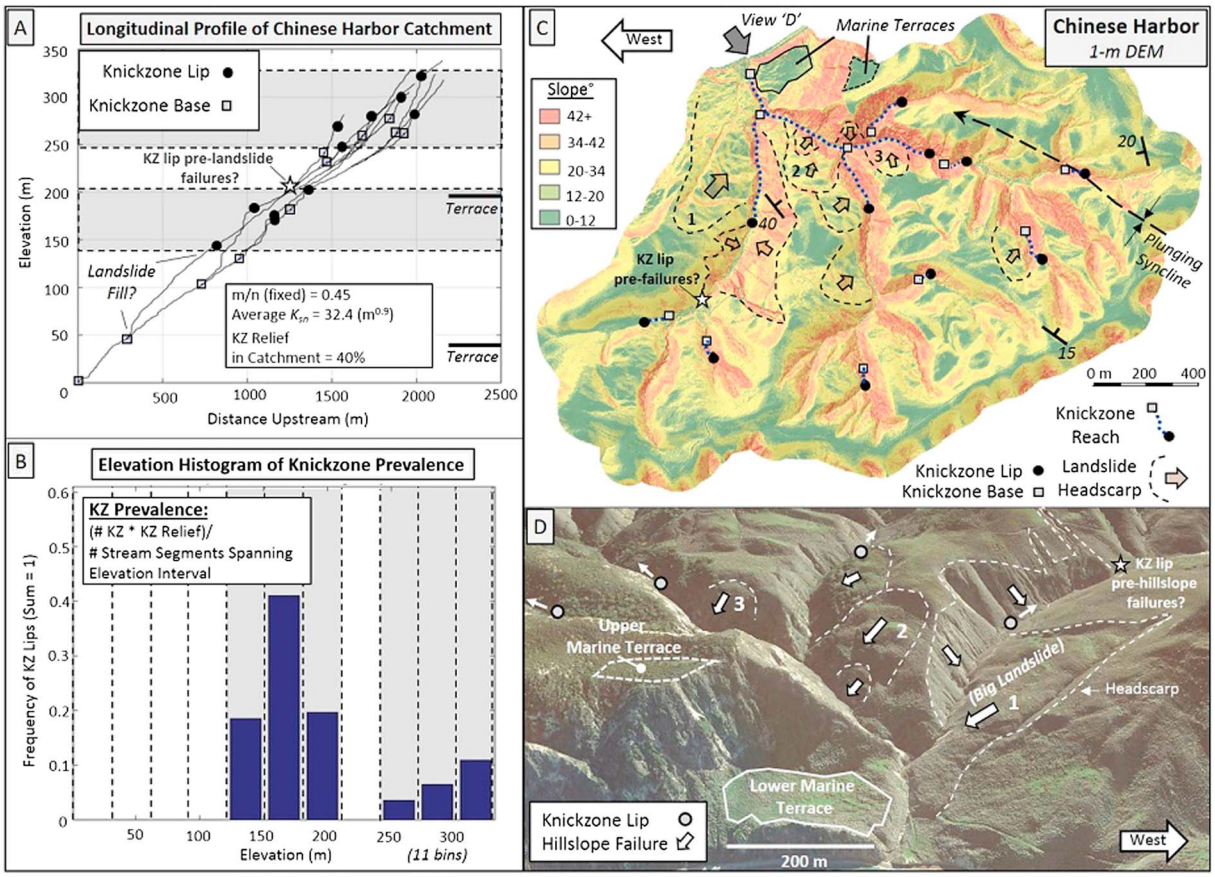

Figure 12. (a) Longitudinal profile of Chinese Harbor catchment (see Figure 5a for location) with mapped knickzones identified by the algorithm. (b) Elevation histogram of knickzone prevalence demonstrates clustering of knickzone lips within two elevation intervals. Gray elevation intervals in Figure 12b are same intervals highlighted in Figure 12a. (c) Slope map of Chinese Harbor plots knickzone lips and bases (connected with white dashed lines), marine terrace platforms, and headscarps of slope failures. Hillslope failures are widespread downstream of knickzones that cluster at ~150–200 m above sea level. (d) Oblique Google Earth© imagery of Chinese Harbor illustrating knickzone lip positions, terrace levels, and hillslope failures. A large landslide and multiple smaller hillslope failures fill the western tributary. We infer the position of this knickzone lip prior to hillslope failure and canyon infilling (white star).

The relations between knickzones and underlying geology can provide preliminary insight into whether or not a landscape is in steady state or where sites of high disequilibrium are located. Such insight reveals whether topography is adjusting toward a new equilibrium over long timescales—an important consideration when modeling and interpreting the rates of surface processes in a particular landscape [e.g., *Scherler et al.*, 2015].

5.1. Algorithm Significance and Potential

Given the 80–90% accuracy to a spatial error of ~50 m in automated knickzone selections on 1, 10, and 30 m DEMs, this algorithm is most suitable as (1) an effective mapping tool to expose topographic breaks within a fluvial network and (2) a data-gathering tool used to compile large data sets to contextualize knickzone position and geometry with respect to regional climate, lithology, and tectonics. We still recommend individual selection of knickzones if investigations require the exact location of knickzone lips and bases [*Whipple et al.*, 2007]; however, manual selection and measurement of knickzones is commonly tedious and limits the size and spatial extent of knickzone maps and data sets. In contrast, the KZ-Picker algorithm essentially removes this limit by compiling all knickzones within a landscape in minutes. Although sacrificing some accuracy, the potential to map knickzones over a large spatial range by the KZ-Picker algorithm provides a new approach to characterize the dynamics of transient landscapes and can inform where manual knickzone selection techniques are inconsistent. Rapid automated knickzone mapping aids development of

preliminary interpretations and testable hypotheses. Moreover, mapping can quickly highlight interesting portions of a landscape that may merit more detailed manual knickzone selection and investigation.

5.2. Application to Inform Models of Knickzone Migration

Large data sets of mapped knickzone features can be used to address outstanding questions in landscape evolution, particularly how landscape adjustment itself is impacted by variations in catchment hydrology, tectonic deformation, lithologic characteristics, or rates of base-level fall. Knickzone migration commonly dictates the pace of landscape adjustment to changing boundary conditions [e.g., *Whipple and Tucker*, 1999; *Whipple*, 2001]. Yet the dynamics of incision processes in knickzone reaches are poorly understood across various hydrologic, tectonic, and geologic settings [*Whipple*, 2004; *DiBiase et al.*, 2015]. This uncertainty limits our ability to produce informed models of knickzone erosion and upstream migration and can reduce confidence when interpreting the spatial distribution of knickzones across a landscape.

The most widely used knickzone-retreat models consider upstream-contributing drainage area as a proxy for sediment and water discharge and use drainage area as the main dependent variable that impacts knickzone retreat rate [e.g., *Crosby and Whipple*, 2006; *Berlin and Anderson*, 2007; *Loget and Van Den Driessche*, 2009]. In graded, steady-state reaches, slope and drainage area can be more directly related to bed shear stress than in steep reaches where flow dynamics and erosional process are more variable [*Lamb et al.*, 2015]. Although still modeled primarily as a function of upstream drainage area, coefficients relating drainage area to knickzone retreat rate span more than five orders of magnitude in a compilation of 15 studies [*Loget and Van Den Driessche*, 2009]. Some of this scatter may reflect a base-level fall control on horizontal knickzone retreat rate if the relationship between erosion and channel slope is nonlinear [*Whipple*, 2001; *Niemann et al.*, 2001; *Whittaker and Boulton*, 2012], but many studies still indicate a wide range of knickzone retreat efficiency. Efforts to understand landscape response to base-level fall should evaluate whether variation in the relationship between retreat rate and drainage area in different study sites reflects contrasts in rock type, catchment hydrology, or process transitions that may occur when transitioning from vertical streambed incision to more horizontal knickzone retreat.

To refine and improve knickzone retreat models, large data sets of knickzone positions and geometries gathered using the algorithm introduced here can serve as reference data sets to compare to knickzone positions predicted from either stream-power or sediment-flux-driven retreat models [*Wobus et al.*, 2006a; *Gasparini et al.*, 2007; *Crosby et al.*, 2007; *Royden and Perron*, 2013]. Residuals between the model predictions and knickzone positions mapped with the KZ-Picker could highlight additional controls on knickzone migration that may stem from spatial differences in the strength of exhumed bedrock [*DiBiase et al.*, 2015], boulder armoring at the base of waterfalls [*DiBiase et al.*, 2015; *Shobe et al.*, 2016; *Bennett et al.*, 2016], variations in upstream supply of coarse bedload [*Cowie et al.*, 2008; *Jansen et al.*, 2011; *Brocard et al.*, 2016], divide migration initiated from differential rates of upstream knickzone migration in neighboring watersheds [*Gilbert*, 1909; *Willett et al.*, 2014; *Whipple et al.*, 2017], or changes in erosional processes within knickzone reaches, such as block toppling or undercutting [*Lamb et al.*, 2015]. These factors are quantified in few landscapes but have been argued to support strong spatial contrasts in topographic form and allow surface uplift of relict topography to persist over million year timescales in some settings [*Wobus et al.*, 2006c; *Willett et al.*, 2014; *DiBiase et al.*, 2015; *Brocard et al.*, 2016; *Bennett et al.*, 2016].

Feedbacks between sediment flux, erosional process, and stream incision occurring during knickzone migration are rarely considered in landscape-scale knickzone retreat models due to their complex temporal or spatial behavior [e.g., *Gasparini et al.*, 2007]. Particularly, transient conditions and knickzone formation may be required to exceed certain stability thresholds of erosional processes that are maintained in steady-state landscapes. For example, knickzone formation may cause the dominant incision process to change from abrasion to undercutting and toppling [*Lamb et al.*, 2015], trigger rapid hillslope failure and boulder armoring at the base of waterfalls [*DiBiase et al.*, 2015; *Golly et al.*, 2017], or drive inward divide migration in perched relict landscapes through discrete river capture events [*Willett et al.*, 2014]. The interaction of these processes to influence landscape evolution is amplified in transient landscapes and could either stall or accelerate knickzone migration specifically in regions where certain thresholds have been exceeded and process transitions have taken place. Such temporal or spatial heterogeneity in knickzone retreat rate can be complicated to model or predict but may be an important driver of large stream-capture events [*Bishop*, 1995; *Prince et al.*, 2011; *Willett et al.*, 2014] or long-term preservation of hanging valleys [*Wobus et al.*, 2006c]—features that are

challenging to explain in a stream-power framework that assumes a relatively homogeneous landscape [*Crosby et al.*, 2007; *Whipple et al.*, 2017]. In landscapes where such feedbacks are likely operating during knickzone migration, mapping knickzone position and geometry may be the first step to quantifying the significance of interactions among these variables and provide a richer understanding of what controls the rate and style of landscape adjustment to base-level fall under different environmental conditions.

5.3. Application to Hillslope-Channel Coupling and Tectonic Geomorphology

Propagating knickzones provide an ergodic (space-for-time) substitution that highlights how hillslopes respond to base-level fall [*Bigi et al.*, 2006; *Mudd and Furbish*, 2007; *Hilley and Arrowsmith*, 2008; *Gallen et al.*, 2011]. Detailed analysis of hillslopes downstream and upstream from propagating knickzones can help delineate feedbacks between hillslope processes and changes in channel incision rate. Key uncertainties include (1) how landscapes transition from soil-mantled to mixed- and bare-bedrock hillslopes [*DiBiase et al.*, 2012]; (2) what conditions cause landscapes to reach a threshold-hillslope angle where hillslope gradient decouples from erosion rate [*Burbank et al.*, 1996; *Binnie et al.*, 2007; *Larsen and Montgomery*, 2012; *DiBiase et al.*, 2012]; and (3) how soil nutrient content, vegetation cover, and grain size change in response to incision and hillslope steepening [*Attal et al.*, 2015; *Milodowski et al.*, 2015]. This new algorithm locates knickzones across full watersheds or entire regions, enabling studies that connect hillslopes response to knickzone migration over wide spatial scales, thereby offering a complimentary approach to site-specific investigations.

More generally, when paired with the mapping capabilities of the KZ-Picker, the global coverage of DEMs will likely lead to the discovery and quantification of many unrecognized features and landscape discontinuities commonly associated with knickzone occurrence [*Wobus et al.*, 2006b]. These features could be active faults [*Kirby and Whipple*, 2012; *Whittaker and Walker*, 2015], stream-capture events [*Prince et al.*, 2011; *Willett et al.*, 2014], changes in rock-uplift rates [*Clark et al.*, 2005; *Hilley and Arrowsmith*, 2008], or strong contrasts in erosional efficiency [*Weissel and Seidl*, 1997; *Brocard and Van der Beek*, 2006]. The presence or absence of such features in a region could indicate whether tectonic deformation and subsequent landscape response occurs in episodic events or in a more continuous fashion. Such insights may have further implications related to the mechanics of crustal deformation underlying a particular landscape, the seismicity of a region, or the manner in which a land surface is lowered following tectonic uplift, e.g., through steady vertical incision or horizontal knickzone migration [*Seidl et al.*, 1994; *Whipple*, 2004]. To address these problems requires a large-scale contextualization of knickzones with surrounding geology, climate, and lithology—a process which is enabled by increasing availability of reliable DEMs and an automated knickzone selection algorithm that can efficiently process digital topographic data.

6. Conclusion

We present a new computer algorithm (KZ-Picker) that uses a fully automated system to process DEM grids, map the position of knickzone features, and measure knickzone dimensions. We analyze stream profiles in χ-space, which facilitates the identification and quantification of knickzones by representing these features as departures from a steady-state channel profile. We detail a preprocessing routine necessary to remove noise from raw DEM-derived stream networks and define the scale of knickzone features of interest. We then identify optimal parameter values for commonly used DEM resolutions: 1 m, 10 m, and 30 m. We quantify the uncertainty of automated knickzone selections on these DEMs by comparing algorithm results to individually selected knickzone boundaries based on a 1 m resolution DEM of six 1.7–6.1 km^2 catchments on Santa Cruz Island, California. For the 1 m DEM, ~93% of the 178 manually selected knickzone boundaries match algorithm-selected knickzone boundaries within a spatial tolerance of 100 m, 88% to within 50 m, and 46% to within 10 m. About 9% of algorithm-selected knickzones are spurious (not within 50 m of a calibration knickzone), and measurements of knickzone height have an average uncertainty of $<$10%. Using 10 and 30 m DEMs, automated knickzone selections have similar accuracy, but as DEM resolution coarsens and smooths topography, calibration knickzones commonly move tens of meters or become hidden relative to calibration knickzones selected on the 1 m DEM. KZ-Picker significantly reduces processing time by orders of magnitude compared to manual knickzone-selection techniques, given that it maps and measures $>$170 knickzones in a ~10,000 $\times$ 10,000 DEM in a few minutes of runtime. This efficiency enables characterization of transient landscape dynamics and discoveries of disequilibrium features associated with knickzones, including active faults, stream-capture events, or strong spatial contrasts in rock strength or erosional efficiency.

Appendix A

Table A1. Suggested Parameter Values From Additional Preliminary Case Studies[a]

Location	DEM Res.	Relief (m)	Drainage Area (km^2)	Smoothing Window	Lumping Window	Min KZ Prelumping	Min KZ Postlumping	Additional Notes
Santa Cruz Island	1 m	~500	1.7–6.1	125 cells, *polynomial order* = 11	75 m	1 m	5 m (mag)	Landscape-scale knickzones (>100 m)
Santa Cruz Island	1 m	~500	1.7–6.1	85 cells, *polynomial order* = 11	20 m	0.25 m	2 m (mag)	Sharper knickzone steps (10–100 m)
Santa Cruz Island	10 m	~500	1.7–6.1	None	75 m	0.5 m	5 m (mag)	Landscape-scale knickzones (>100 m)
Santa Cruz Island	30 m	~500	1.7–6.1	None	100 m	0.5 m	5 m (mag)	Landscape-scale knickzones (>100 m)
N. San Jacinto Mtns. Drainage Area > 0.1 km^2	1 m	~2300	9–27	101 cells, *polynomial order* = 11	30 m	1.5 m	20 m (mag)	Landscape-scale knickzones (>100 m)
E. San Gabriel Mtns. Drainage Area > 0.1 km^2	1 m	~2200	8–27	101 cells, *polynomial order* = 11	30 m	1.5 m	20 m (mag)	Landscape-scale knickzones (>100 m)
Taiwan (nearly all mountainous terrain: Drainage area > 1 km^2)	40 m	~3900	118–1021	17 cells, *polynomial order* = 3	210 m (~5 cells)	10 m	20 m (mag)	Coarse DEM requires more smoothing if not generated by subsampling high-res. DEM

[a](mag) denotes that knickzone magnitude rather than relief as the measure used to filter small knickzones.

Acknowledgments
The Matlab-based algorithm for this work is available on the Community Surface Dynamics Modeling Systems (CSDMS) website in the Terrestrial Tools section called KZ-Picker and at https://github.com/UP-RS-ESP/DEM-KPP. We thank the National Center for Airborne Laser Mapping (NCALM) and the USGS for creating the lidar topographic data set of the California Channel Islands. This work was supported by the NSF Geomorphology Land Use Dynamics program through NSF grant EAR-1148268. Part of this investigation was carried out with funds by the German Federal Ministry of Education and Research provided to the PROGRESS initiative. We are pleased to thank Leal Anne Kerry Mertes, Lloyd Edwards, and Mary Edwards for scholarship contributions to A.B.N., and in the future, A.B.N. hopes to replicate their generosity toward young enthusiastic scientists. We thank Lyndal Laughrin of the UC field-reserve research network for organizing fieldwork logistics. Simon Mudd, Charlie Shobe, and three anonymous reviewers provided detailed and thoughtful reviews which improved the quality of this manuscript. We thank Roman DiBiase for a stimulating discussion about theoretical predictions of river profile adjustment during transient landscape evolution. Oliver Chadwick, Nina Bingham, and Paul Alessio also provided valuable insight during preliminary fieldwork.

References

Attal, M., S. M. Mudd, M. D. Hurst, B. Weinman, K. Yoo, and M. Naylor (2015), Impact of change in erosion rate and landscape steepness on hillslope and fluvial sediments grain size in the Feather River basin (Sierra Nevada, California), *Earth Surf. Dyn.*, *3*, 201–222.

Baldwin, J. A., Whipple, K. X., and G. E. Tucker (2003), Implications of the shear stress river incision model for the timescale of postorogenic decay of topography, *J. Geophys. Res.*, *108*(B3), 2158, doi:10.1029/2001JB000550.

Berlin, M. M., and R. S. Anderson (2007), Modeling of knickpoint retreat on the Roan Plateau, western Colorado, *J. Geophys. Res.*, *112*, F03S06, doi:10.1029/2006JF000553.

Bennett, G. L., S. R. Miller, J. J. Roering, and D. A. Schmidt (2016), Landslides, threshold slopes, and the survival of relict terrain in the wake of the Mendocino Triple Junction, *Geology*, *44*(5), 363–366.

Bigi, A., L. E. Hasbargen, A. Montanari, and C. Paola (2006), Knickpoints and hillslope failures: Interactions in a steady-state experimental landscape, *GSA Spec. Pap.*, *398*, 295–307, doi:10.1130/2006.2398(18).

Binnie, S. A., W. M. Phillips, M. A. Summerfield, and L. K. Fifield (2007), Tectonic uplift, threshold hillslopes, and denudation rates in a developing mountain range, *Geology*, *35*(8), 743–746.

Bishop, P. (1995), Drainage rearrangement by river capture, beheading and diversion, *Prog. Phys. Geogr.*, *19*(4), 449–473.

Bishop, P., T. B. Hoey, J. D. Jansen, and I. L. Artza (2005), Knickpoint recession rate and catchment area: The case of uplifted rivers in Eastern Scotland, *Earth Surf. Processes Landforms*, *30*(6), 767–778.

Brocard, G., and P. Van der Beek (2006), Influence of incision rate, rock strength, and bedload supply on bedrock river gradients and valley-flat widths: Field-based evidence and calibrations from western Alpine rivers (southeast France), *Geol. Soc. Am. Spec. Pap.*, *398*, 101–126.

Brocard, G. Y., J. K. Willenbring, T. E. Miller, and F. N. Scatena (2016), Relict landscape resistance to dissection by upstream migrating knickpoints, *J. Geophys. Res. Earth Surf.*, *121*, 1182–1203, doi:10.1002/2015JF003678.

Burbank, D. W., J. Leland, E. Fielding, R. S. Anderson, N. Brozovic, M. R. Reid, and C. Duncan (1996), Bedrock incision, rock uplift and threshold hillslopes in the northwestern Himalayas, *Nature*, *379*, 505–510.

Chatanantavet, P., and G. Parker (2009), Physically based modeling of bedrock incision by abrasion, plucking, and macroabrasion, *J. Geophys. Res.*, *114*, F04018, doi:10.1029/2008JF001044.

Clark, M. K., G. Maheo, J. Saleeby, and K. A. Farley (2005), The non-equilibrium landscape of the southern Sierra Nevada, California, *GSA Today*, *15*, 4–10.

Clark, M. K., L. H. Royden, K. X. Whipple, B. C. Burchfiel, X. Zhang, and W. Tang (2006), Use of a regional, relict landscape to measure vertical deformation of the eastern Tibetan Plateau, *J. Geophys. Res.*, *111*, F03002, doi:10.1029/2005JF000294.

Clubb, F. J., S. M. Mudd, D. T. Milodowski, M. D. Hurst, and L. J. Slater (2014), Objective extraction of channel heads from high-resolution topographic data, *Water Resour. Res.*, *50*, 4283–4304, doi:10.1002/2013WR015167.

Cowie, P. A., A. C. Whittaker, M. Attal, G. Roberts, G. E. Tucker, and A. Ganas (2008), New constraints on sediment-flux-dependent river incision: Implications for extracting tectonic signals from river profiles, *Geology*, *36*(7), 535–538.

Crosby, B. T., and K. X. Whipple (2006), Knickpoint initiation and distribution within fluvial networks: 236 waterfalls in the Waipaoa River, North Island, New Zealand, *Geomorphology*, *82*(1), 16–38.

Crosby, B. T., K. X. Whipple, N. M. Gasparini, and C. W. Wobus (2007), Formation of fluvial hanging valleys: Theory and simulation, *J. Geophys. Res.*, *112*, F03S10, doi:10.1029/2006JF000566.

DiBiase, R. A., K. X. Whipple, A. M. Heimsath, and W. B. Ouimet (2010), Landscape form and millennial erosion rates in the San Gabriel Mountains, CA, *Earth Planet. Sci. Lett.*, *289*(1), 134–144.

DiBiase, R. A., A. M. Heimsath, and K. X. Whipple (2012), Hillslope response to tectonic forcing in threshold landscapes, *Earth Surf. Processes Landforms*, *37*(8), 855–865.
DiBiase, R. A., K. X. Whipple, M. P. Lamb, and A. M. Heimsath (2015), The role of waterfalls and knickzones in controlling the style and pace of landscape adjustment in the western San Gabriel Mountains, California, *Geol. Soc. Am. Bull.*, *127*(3–4), 539–559, doi:10.1130/B31113.1.
Dubinski, I. M., and E. Wohl (2013), Relationships between block quarrying, bed shear stress, and stream power: A physical model of block quarrying of a jointed bedrock channel, *Geomorphology*, *180*, 66–81.
Duvall, A., E. Kirby, and D. W. Burbank (2004), Tectonic and lithologic controls on bedrock channel profiles and processes in coastal California, *J. Geophys. Res.*, *109*, F03002, doi:10.1029/2003JF000086.
Fisher, G. B., B. Bookhagen, and C. B. Amos (2013), Channel planform geometry and slopes from freely available high-spatial resolution imagery and DEM fusion: Implications for channel width scalings, erosion proxies, and fluvial signatures in tectonically active landscapes, *Geomorphology*, *194*, 46–56.
Flint, J. (1974), Stream gradient as a function of order, magnitude, and discharge, *Water Resour. Res.*, *10*(5), 969–973, doi:10.1029/WR010i005p00969.
Gallen, S. F., K. W. Wegmann, K. L. Frankel, S. Hughes, R. Q. Lewis, N. Lyons, P. Paris, K. Ross, J. B. Bauer, and A. C. Witt (2011), Hillslope response to knickpoint migration in the southern Appalachians: Implications for the evolution of post-orogenic landscapes, *Earth Surf. Processes Landforms*, *36*.
Gardner, T. W. (1983), Experimental study of knickpoint and longitudinal profile evolution in cohesive, homogeneous material, *Geol. Soc. Am. Bull.*, *94*(5), 664–672.
Gasparini, N. M., R. L. Bras, and K. X. Whipple (2006), Numerical modeling of non-steady-state river profile evolution using a sediment-flux-dependent incision model, *Geol. Soc. Am. Spec. Pap.*, *398*, 127–141.
Gasparini, N. M., K. X. Whipple, and R. L. Bras (2007), Predictions of steady state and transient landscape morphology using sediment-flux-dependent river incision models, *J. Geophys. Res.*, *112*, F03S09, doi:10.1029/2006JF000567.
Gilbert, G. K. (1909), The convexity of hilltops, *J. Geol.*, *17*, 344–350.
Godard, V., G. E. Tucker, G. Burch Fisher, D. W. Burbank, and B. Bookhagen (2013), Frequency-dependent landscape response to climatic forcing, *Geophys. Res. Lett.*, *40*, 859–863, doi:10.1002/grl.50253.
Golly, A., J. M. Turowski, A. Badoux, and N. Hovius (2017), Controls and feedbacks in the coupling of mountain channels and hillslopes, *Geology*, doi:10.1130/G38831.1.
Gonga-Saholiariliva, N., Y. Gunnell, D. Harbor, and C. Mering (2011), An automated method for producing synoptic regional maps of river gradient variation: Procedure, accuracy tests, and comparison with other knickpoint mapping methods, *Geomorphology*, *134*(3–4), 394–407.
Hack, J. T. (1957), Studies of longitudinal stream profiles in Virginia and Maryland, *U.S. Geol. Surv. Prof. Pap., 294-B*, 97 pp.
Harbor, D., A. Bacastow, A. Heath, and J. Rogers (2005), Capturing variable knickpoint retreat in the Central Appalachians, USA, *Geogr. Fis. Din. Quat.*, *28*, 23–36.
Harkins, N., E. Kirby, A. Heimsath, R. Robinson, and U. Reiser (2007), Transient fluvial incision in the headwaters of the Yellow River, northeastern Tibet, China, *J. Geophys. Res.*, *112*, F03S04, doi:10.1029/2006JF000570.
Haviv, I., Y. Enzel, K. Whipple, E. Zilberman, J. Stone, A. Matmon, and L. Fifield (2006), Amplified erosion above waterfalls and oversteepened bedrock reaches, *J. Geophys. Res.*, *111*, F04004, doi:10.1029/2006JF000461.
Haviv, I., Y. Enzel, K. Whipple, E. Zilberman, A. Matmon, J. Stone, and K. Fifield (2010), Evolution of vertical knickpoints (waterfalls) with resistant caprock: Insights from numerical modeling, *J. Geophys. Res.*, *115*, F03028, doi:10.1029/2008JF001187.
Heimsath, A. M., W. E. Dietrich, K. Nishiizumi, and R. C. Finkel (1997), The soil production function and landscape equilibrium, *Nature*, *388*(6640), 358–361.
Hilley, G. E., and J. R. Arrowsmith (2008), Geomorphic response to uplift along the Dragon's back pressure ridge, Carrizo plain, California, *Geology*, *36*(5), 367–370.
Howard, A. D., and G. Kerby (1983), Channel changes in badlands, *Geol. Soc. Am. Bull.*, *94*(6), 739–752.
Howard, A. D., W. E. Dietrich, and M. A. Seidl (1994), Modeling fluvial erosion on regional to continental scales, *J. Geophys. Res.*, *99*, 13,971–13,986, doi:10.1029/94JB00744.
Hurst, M. D., S. M. Mudd, R. Walcott, M. Attal, and K. Yoo (2012), Using hilltop curvature to derive the spatial distribution of erosion rates, *J. Geophys. Res.*, *117*, F02017, doi:10.1029/2011JF002057.
Jansen, J. D., D. Fabel, P. Bishop, S. Xu, C. Schnabel, and A. T. Codilean (2011), Does decreasing paraglacial sediment supply slow knickpoint retreat?, *Geology*, *39*(6), 543–546.
Kirby, E., and K. X. Whipple (2012), Expression of active tectonics in erosional landscapes, *J. Struct. Geol.*, *44*, 54–75.
Korup, O. (2006), Rock-slope failure and the river long profile, *Geology*, *34*(1), 45–48.
Lague, D. (2014), The stream power river incision model: Evidence, theory and beyond, *Earth Surf. Processes Landforms*, *39*(1), 38–61.
Lamb, M. P., and W. E. Dietrich (2009), The persistence of waterfalls in fractured rock, *Geol. Soc. Am. Bull.*, *121*(7–8), 1123–1134.
Lamb, M. P., A. D. Howard, W. E. Dietrich, and J. T. Perron (2007), Formation of amphitheater-headed valleys by waterfall erosion after large-scale slumping on Hawai'i, *Geol. Soc. Am. Bull.*, *119*(7–8), 805–822.
Lamb, M. P., N. J. Finnegan, J. S. Scheingross, and L. S. Sklar (2015), New insights into the mechanics of fluvial bedrock erosion through flume experiments and theory, *Geomorphology*, *244*, 33–55.
Larsen, I. J. and D. R. Montgomery (2012), Landslide erosion coupled to tectonics and river incision, *Nat. Geosci.*, *5*, 468–473.
Loget, N., and J. Van Den Driessche (2009), Wave train model for knickpoint migration, *Geomorphology*, *106*(3), 376–382.
Mackey, B. H., J. S. Scheingross, M. P. Lamb, and K. A. Farley (2014), Knickpoint formation, rapid propagation, and landscape response following coastal cliff retreat at the last interglacial sea-level highstand: Kaua'i, Hawai'i, *Geol. Soc. Am. Bull.*, *126*(7–8), 925–942.
Marshall, J. A., and J. J. Roering (2014), Diagenetic variation in the Oregon Coast Range: Implications for rock strength, soil production, hillslope form, and landscape evolution, *J. Geophys. Res. Earth Surf.*, *119*, 1395–1417, doi:10.1002/2013JF003004.
Meyer-Peter, E., and R. Müller (1948), Formulas for bed-load transport, in *Proceedings of the 2nd Meeting of the International Association for Hydraulic Structures Research, Inter. Assoc. for Hydraul. Res.*, pp. 39–64, Delft, Netherlands.
Miller, S. R., S. L. Baldwin, and P. G. Fitzgerald (2012), Transient fluvial incision and active surface uplift in the Woodlark Rift of eastern Papua New Guinea, *Lithosphere*, *4*(2), 131–149.
Miller, S. R., P. B. Sak, E. Kirby, and P. R. Bierman (2013), Neogene rejuvenation of central Appalachian topography: Evidence for differential rock uplift from stream profiles and erosion rates, *Earth Planet. Sci. Lett.*, *369*, 1–12.
Milodowski, D. T., S. M. Mudd, and E. T. Mitchard (2015), Erosion rates as a potential bottom-up control of forest structural characteristics in the Sierra Nevada Mountains, *Ecology*, *96*(1), 31–38.

Montgomery, D. R., and E. Foufoula-Georgiou (1993), Channel network source representation using digital elevation models, *Water Resour. Res.*, *29*(12), 3925–3934, doi:10.1029/93WR02463.
Moon, S., C. P. Chamberlain, K. Blisniuk, N. Levine, D. H. Rood, and G. E. Hilley (2011), Climatic control of denudation in the deglaciated landscape of the Washington cascades, *Nat. Geosci.*, *4*(7), 469–473.
Mudd, S. M., and D. J. Furbish (2007), Responses of soil-mantled hillslopes to transient channel incision rates, *J. Geophys. Res.*, *112*, F03S18, doi:10.1029/2006JF000516.
Mudd, S. M., M. Attal, D. T. Milodowski, S. W. Grieve, and D. A. Valters (2014), A statistical framework to quantify spatial variation in channel gradients using the integral method of channel profile analysis, *J. Geophys. Res. Earth Surf.*, *119*, 138–152, doi:10.1002/2013JF002981.
Muhs, D. R., K. R. Simmons, R. R. Schumann, L. T. Groves, S. B. DeVogel, S. A. Minor, and D. Laurel (2014), Coastal tectonics on the eastern margin of the Pacific Rim: Late Quaternary sea-level history and uplift rates, Channel Islands National Park, California, USA, *Quat. Sci. Rev.*, *105*, 209–238.
Muller, E. H. (1977), Late glacial and early postglacial environments in western New York, *Ann. N. Y. Acad. Sci.*, *288*(1), 223–233.
Niemann, J. D., N. M. Gasparini, G. E. Tucker, and R. L. Bras (2001), A quantitative evaluation of Playfair's law and its use in testing long-term stream erosion models, *Earth Surf. Processes Landforms*, *26*, 1317–1332.
Orfanidis, S. J. (1996), *Introduction to Signal Processing*, *Prentice Hall*, Englewood Cliffs, N. J.
Orlandini, S., P. Tarolli, G. Moretti, and G. Dalla Fontana (2011), On the prediction of channel heads in a complex alpine terrain using gridded elevation data, *Water Resour. Res.*, *47*, W02538, doi:10.1029/2010WR009648.
Perron, J. T., and L. Royden (2013), An integral approach to bedrock river profile analysis, *Earth Surf. Processes Landforms*, *38*(6), 570–576.
Pinter, N., S. B. Lueddecke, E. A. Keller, and K. R. Simmons (1998), Late quaternary slip on the Santa Cruz Island fault, California, *Geol. Soc. Am. Bull.*, *110*(6), 711–722.
Prince, P. S., J. A. Spotila, and W. S. Henika (2011), Stream capture as driver of transient landscape evolution in a tectonically quiescent setting, *Geology*, *39*(9), 823–826.
Purinton, B., and B. Bookhagen (2017), Validation of digital elevation models (DEMs) and comparison of geomorphic metrics on the southern Central Andean Plateau, *Earth Surf. Dyn.*, *5*, 211–237, doi:10.5194/esurf-5-211-2017.
Queiroz, G., L. E. Salamuni, and E. R. Nascimento (2015), Knickpoint finder: A software tool that improves neotectonic analysis, *Comput. Geosci.*, *76*, 80–87.
Royden, L. H., M. K. Clark, and K. X. Whipple (2000), Evolution of river elevation profiles by bedrock incision: Analytical solutions for transient river profiles related to changing uplift and precipitation rates, *Eos Trans. AGU*, *81*, 48.
Royden, L., and T. J. Perron (2013), Solutions of the stream power equation and application to the evolution of river longitudinal profiles, *J. Geophys. Res. Earth Surf.*, *118*, 497–518, doi:10.1002/jgrf.20031.
Scherler, D., B. Bookhagen, H. Wulf, F. Preusser, and M. R. Strecker (2015), Increased late Pleistocene erosion rates during fluvial aggradation in the Garhwal Himalaya, northern India, *Earth Planet. Sci. Lett.*, *428*, 255–266.
Schoenbohm, L. M., K. X. Whipple, B. C. Burchfiel, and L. Chen (2004), Geomorphic constraints on surface uplift, exhumation, and plateau growth in the Red River region, Yunnan Province, China, *Geol. Soc. Am. Bull.*, *116*(7–8), 895–909.
Schwanghart, W., and D. Scherler (2014), Short communication: TopoToolbox 2–MATLAB-based software for topographic analysis and modeling in Earth surface sciences, *Earth Surf. Dyn.*, *2*(1), 1–7.
Seidl, M. A., and W. E. Dietrich (1992), The problem of channel erosion into bedrock, *Funct. Geomorphol.*, *23*, 101–124.
Seidl, M. A., W. E. Dietrich, and J. W. Kirchner (1994), Longitudinal profile development into bedrock: An analysis of Hawaiian channels, *J. Geol.*, 457–474.
Shobe, C. M., G. E. Tucker, and R. S. Anderson (2016), Hillslope-derived blocks retard river incision, *Geophys. Res. Lett.*, *43*, 5070–5078, doi:10.1002/2016GL069262.
Sklar, L. S., and W. E. Dietrich (2001), Sediment and rock strength controls on river incision into bedrock, *Geology*, *29*(12), 1087–1090.
Sklar, L. S., and W. E. Dietrich (2004), A mechanistic model for river incision into bedrock by saltating bed load, *Water Resour. Res.*, *40*, W06301, doi:10.1029/2003WR002496.
Smith, M. W. (2014), Roughness in the earth sciences, *Earth Sci. Rev.*, *136*, 202–225.
Snyder, N. P., K. X. Whipple, G. E. Tucker, and D. J. Merritts (2000), Landscape response to tectonic forcing: Digital elevation model analysis of stream profiles in the Mendocino triple junction region, northern California, *Geol. Soc. Am. Bull.*, *112*(8), 1250–1263.
Snyder, N. P., K. X. Whipple, G. E. Tucker, and D. J. Merritts (2002), Interactions between onshore bedrock-channel incision and nearshore wave-base erosion forced by eustasy and tectonics, *Basin Res.*, *14*(2), 105–127.
Tucker, G. E. and K. X. Whipple (2002), Topographic outcomes predicted by stream erosion models: Sensitivity analysis and intermodel comparison. *J. Geophys. Res.*, *107*(B9), 2179, doi:10.1029/2001JB000162.
Wang, Y., H. Zhang, D. Zheng, J. Yu, J. Pang, and Y. Ma (2017), Coupling slope-area analysis, integral approach and statistic tests to steady-state bedrock river profile analysis, *Earth Surf. Dyn.*, *5*, 145–160, doi:10.5194/esurf-5-145-2017.
Weaver, D., and B. Nolf (1969), Geology of Santa Cruz Island (map). Geology of the northern Channel Islands, southern California borderland: *Pacific Section, American Association of Petroleum Geologists Special Publication*, scale, 1(24), 000.
Weissel, J. K., and M. A. Seidl (1997), Influence of rock strength properties on escarpment retreat across passive continental margins, *Geology*, *25*(7), 631–634.
Whipple, K. X., and G. E. Tucker (1999), Dynamics of the stream-power river incision model: Implications for height limits of mountain ranges, landscape response timescales, and research needs, *J. Geophys. Res.*, *104*, 17,661–17,674, doi:10.1029/1999JB900120.
Whipple, K. X., G. S. Hancock, and R. S. Anderson (2000), River incision into bedrock: Mechanics and relative efficacy of plucking, abrasion, and cavitation, *Geol. Soc. Am. Bull.*, *112*(3), 490–503.
Whipple, K. X. (2001), Fluvial landscape response time: How plausible is steady-state denudation?, *Am. J. Sci.*, *301*(4–5), 313–325.
Whipple, K. X. (2004), Bedrock rivers and the geomorphology of active orogens, *Annu. Rev. Earth Planet. Sci.*, *32*, 151–185.
Whipple, K. X., C. Wobus, B. Crosby, E. Kirby, and D. Sheehan (2007), New tools for quantitative geomorphology: Extraction and interpretation of stream profiles from digital topographic data, *GSA Short Course*, *506*.
Whipple, K. X. (2009), The influence of climate on the tectonic evolution of mountain belts, *Nat. Geosci.*, *2*(2), 97–104.
Whipple, K. X., R. A. DiBiase, and B. T. Crosby (2013), Bedrock Rivers, in *Treatise on Geomorphology*, vol. 9, edited by J. Shroder, Jr., and E. Wohl, Academic Press, San Diego, Calif., doi:10.1016/B978-0-12-374739-6.00254-2.
Whipple, K. X., A. M. Forte, R. A. DiBiase, N. M. Gasparini, and W. B. Ouimet (2017), Timescales of landscape response to divide migration and drainage capture: Implications for the role of divide mobility in landscape evolution, *J. Geophys. Res. Earth Surf.*, *122*, 248–273, doi:10.1002/2016JF003973.

Whittaker, A. C. (2012), How do landscapes record tectonics and climate? *Lithosphere*, *4*(2), 160–164.
Whittaker, A. C., and S. J. Boulton (2012), Tectonic and climatic controls on knickpoint retreat rates and landscape response times, *J. Geophys. Res.*, *117*, F02024, doi:10.1029/2011JF002157.
Whittaker, A. C., and A. S. Walker (2015), Geomorphic constraints on fault throw rates and linkage times: Examples from the Northern Gulf of Evia, Greece, *J. Geophys. Res. Earth Surf.*, *120*, 137–158, doi:10.1002/2014JF003318.
Whittaker, A. C., P. A. Cowie, M. Attal, G. E. Tucker, and G. P. Roberts (2007), Bedrock channel adjustment to tectonic forcing: Implications for predicting river incision rates, *Geology*, *35*(2), 103–106.
Willett, S. D., S. W. McCoy, J. T. Perron, L. Goren, and C. Y. Chen (2014), Dynamic reorganization of river basins, *Science*, *343*(6175) 1248765.
Wobus, C., K. X. Whipple, E. Kirby, N. Snyder, J. Johnson, K. Spyropolou, B. Crosby, and D. Sheehan (2006a), Tectonics from topography: Procedures, promise, and pitfalls, *Geol. Soc. Am. Spec. Pap.*, *398*, 55–74.
Wobus, C. W., K. X. Whipple, and K. V. Hodges (2006b), Neotectonics of the central Nepalese Himalaya: Constraints from geomorphology, detrital 40Ar/39Ar thermochronology, and thermal modeling, *Tectonics*, *25*, TC4011, doi:10.1029/2005TC001935.
Wobus, C. W., B. T. Crosby, and K. X. Whipple (2006c), Hanging valleys in fluvial systems: Controls on occurrence and implications for landscape evolution, *J. Geophys. Res.*, *111*, TC4011, doi:10.1029/2005TC001935.
Wobus, C. W., G. E. Tucker, and R. S. Anderson (2010), Does climate change create distinctive patterns of landscape incision?, *J. Geophys. Res.*, *115*, F04008, doi:10.1029/2009JF001562.